Fatigue performance simulation of reinforced concrete beams externally strengthened with side bonded CFRP sheets

Engineering Structures 316 (2024) 118530

Contents lists available at ScienceDirect

Engineering Structures

journal homepage: www.elsevier.com/locate/engstruct

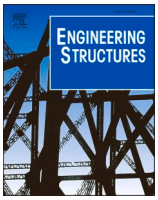

Fatigue performance simulation of reinforced concrete beams externally strengthened with side bonded CFRP sheets

Chuanlong Zou [a,b], Zainah Ibrahim [a,*], Huzaifa Hashim [a], Qing Quan Liang [c,*], Pouria Ayough [d,*], Mohammed Jameel [e]

[a] Department of Civil Engineering, Faculty of Engineering, Universiti Malaya, 50603 Kuala Lumpur, Malaysia
[b] College of Architecture and Civil Engineering, Nanning University, 530200 Nanning, China
[c] College of Sport, Health, and Engineering, Victoria University, PO Box 14428, Melbourne, VIC 8001, Australia
[d] School of Civil Engineering, Chongqing University, Chongqing 400045, China
[e] Department of Civil Engineering, King Khalid University, Abha 62217, Saudi Arabia

ARTICLE INFO

Keywords:
CFRP-concrete interface
Fatigue performance
Finite element simulation
Side-bonded CFRP sheets

ABSTRACT

Damaged Reinforced Concrete (RC) beams are commonly strengthened by bonding Carbon Fiber Reinforced Polymer (CFRP) strips to their soffits. However, inaccessible or narrow soffits limit the use of bottom-bonded CFRP strips. The Side Bonded (SB) CFRP technique overcomes this, yet studies on SB-CFRP-reinforced beams' fatigue behavior are limited. This paper presents a Finite Element (FE) model for simulating the fatigue behavior of RC beams externally strengthened with SB-CFRP sheets. The model incorporates cyclic-dependent CFRP-concrete interface degradation. Existing experimental results are utilized to validate its accuracy. Computational analyses are undertaken to explore the effects of CFRP dimensions, load and prestress levels, and end-U-shaped wrapping on fatigue performance. A simple model is proposed to predict fatigue life considering load and prestress levels. The FE model effectively predicts fatigue performance. Parametric studies indicate that narrow CFRP strips are unable to prevent concrete failure under high loads. Fatigue failure modes include rebar ruptures and CFRP delamination. Besides, the end-U-shaped wrapping reduces interface damage, extending fatigue life. The study emphasizes the sensitivity of vibration excitation method to CFRP debonding. The proposed equation efficiently predicts the fatigue life of RC beams with externally bonded CFRP strips on their sides.

1. Introduction

For over thirty years, Carbon Fiber Reinforced Polymer (CFRP) sheets have been extensively utilized to strengthen or retrofit reinforced concrete (RC) structures. Numerous studies underscore their notable advantages, such as a remarkable strength-to-weight ratio [1], adaptability to environmental conditions [2], minimal thermal expansion [3], and excellent fatigue resistance [4]. The externally bonded (EB) CFRP method stands out as the preferred approach among various strengthening techniques due to its straightforwardness [5]. Mahal et al. [6] conducted a comprehensive investigation into the effectiveness of strengthening RC beams using the EB-CFRP method, examining specimens subjected to both monotonic and fatigue loads. Their findings indicated that this strengthening method enhances the fatigue performance of RC beams by enabling them to endure applied fatigue loads following the rupture of steel reinforcing bars. The primary failure mode observed in beams under fatigue loading was intermediate debonding at the point of steel bar rupture. Generally, the stiffness of the beams experienced a gradual decrease in post-peak range, leading to ductile failure. This observed premature debonding failure mode of strengthened RC beams agrees with the findings of Oehlers et al. [7], who also emphasized the efficacy of retrofitting RC beams using the EB-CFRP method.

Lin et al. [8] focused their attention on CFRP-strengthened RC beams within subtropical highway bridges. They proposed an experimental method that considered the combined impact of hot-wet environmental conditions and random vehicle loads on fatigue behavior. Their observations indicate that the influence of random vehicle loads on the environmental fatigue failure mode of strengthened beams primarily manifested in concrete crack distributions and main reinforcement fracture morphology. Compared to constant amplitude fatigue loads, under random vehicle loads, the strengthened RC beams exhibited fewer

* Corresponding authors.
E-mail addresses: zainah@um.edu.my (Z. Ibrahim), Qing.Liang@vu.edu.au (Q.Q. Liang), pouriaayough@cqu.edu.cn (P. Ayough).

https://doi.org/10.1016/j.engstruct.2024.118530
Received 15 January 2024; Received in revised form 15 April 2024; Accepted 26 June 2024
Available online 4 July 2024

fatigue cracks, which were sparsely distributed.

Chou et al. [9] conducted tests on fourteen RC beams with pre-stressed near-surface-mounted (NSM) CFRP strips under both static and fatigue loading conditions. Concrete cover separation emerged as the predominant failure mode, attributed to factors such as plate end bending moment, shear force, and concentrated stress resulting from small bond lengths, large load amplitudes, and significant prestressing forces. Unlike previous studies [6–8], no CFRP-concrete interfacial debonding was observed in this investigation. By examining NSM CFRP prestressing levels ranging from 0 to 60 %, Oudah and El-Hacha [10,11] concluded that prestressing levels exceeding 20 % could enhance interfacial bonding capacity, leading to well-bonded prestressed specimens while non-prestressed samples experienced debonding. However, Yost et al. [12] reported contrasting results, noting no interfacial debonding in any of the non-prestressed specimens. Quattlebaum et al. [13] determined that concrete beams strengthened with NSM CFRP failed primarily due to reinforcement fracture, regardless of fatigue load amplitude. Similarly, Wahab et al. [14] found that high load amplitudes induced interfacial debonding, while lower amplitudes resulted in reinforcement fracture. Song and Yu [15] investigated the fatigue performance of corroded RC beams reinforced with CFRP sheets through experimental and analytical means. They highlighted that the fatigue behavior of the beams was primarily dictated by the corroded steel bars. The failures were attributed to steel reinforcement rupture in both unstrengthened and CFRP-strengthened beams, thus emphasizing the role of CFRP sheets in maintaining structural integrity.

CFRP sheets have been widely employed to strengthen RC beams under flexural loading by adhering them externally to the undersides of the beams [2,16–20]. However, practical constraints often impede the viability of this method, particularly when the beam's underside is narrow or difficult to access. Notably, the lateral surfaces of beams are often more readily accessible than their undersides in certain scenarios. The width of RC beams is typically constrained by architectural considerations, such as the presence of masonry partitions along beam axes. Consequently, accessing the undersides of beams may be impractical during building operations, especially if masonry blocks beneath them cannot be removed. Additionally, in cases like double-tee slabs, beam widths may not allow for sufficient application of CFRP sheets to meet strength requirements. Adopting a side-bonded approach for strengthening RC beams with CFRP composite sheets resolves numerous practical challenges encountered in construction, including reinforcing double-tee slabs with narrow webs and addressing inaccessible beam undersides due to existing, immovable masonry blocks. Moreover, the narrowness of RC beam undersides in residential structures often limits the CFRP sheet area that can be applied [21]. Consequently, the side-bonded (SB) CFRP (SB-CFRP) technology is a viable solution for rehabilitating damaged beams. Despite its promise, research on the fatigue performance of RC beams strengthened with SB-CFRP sheets remains scarce, highlighting the need for further investigation and practical validation.

Salama et al. [21] and Li et al. [22] investigated the flexural capacity of RC beams strengthened using SB-CFRP sheets, comparing their performance to beams strengthened with conventional bottom-bonded (BB) CFRP (BB-CFRP) systems. Both techniques demonstrated similar effects on flexural stiffness, with the increase in flexural strength ranging from 62 % to 92 % for BB-CFRP-strengthenedbeams and 39.7 % to 93.4 % for SB-CFRP-strengthened specimens. In general, most strengthened beams exhibited steel yielding prior to CFRP debonding from adjacent concrete surfaces. Some specimens experienced steel yielding and minor concrete crushing, followed by CFRP debonding at the failure load.

Hawileh et al. [23] utilized finite element (FE) models to analyze the flexural behavior of RC beams reinforced with SB-CFRP laminates. While an increase in stiffness and load-carrying capacity was noted for SB-CFRP-strengthened beams, this enhancement was accompanied by a reduction in ductility. Hosen et al. [24] examined the effectiveness of Side Near Surface Mounted (SNSM) steel bars and CFRP bars in improving the flexural performance of RC beams. The results demonstrated that the SNSM technology markedly enhanced flexural performance while SB-CFRP bars outperformed steel bars. SB-CFRP-reinforced beams exhibited 2.2 times higher cracking loads, similar yield loads, and 1.4 times higher ultimate capacities than the control beams.

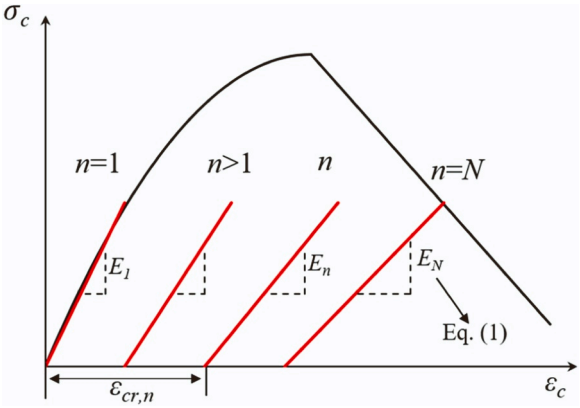

Fig. 1. Stress-stain relationship for concrete under cyclic fatigue loading [30,37].

The preceding discussion highlights the extensive examination of the static behavior of SB-CFRP-strengthened beams, yet there remains a notable gap in understanding the fatigue characteristics of structures reinforced with SB-CFRP. Unlike static loading scenarios, cyclic loading, even at lower intensities, can precipitate catastrophic failures [25,26]. Hence, there is a critical need to investigate the fatigue response of SB-CFRP-strengthened structures under cyclic loading conditions. This study addresses this gap by analyzing the fatigue response of RC beams strengthened with SB-CFRP strips by using a 3D FE model developed using ABAQUS. The simulation model integrates a novel representation of cyclic loading-dependent CFRP-concrete interface bond-slip behavior and nonlinear material properties. Comparative analysis of static and fatigue responses against experimental data is conducted. Furthermore, the FE model is used to explore the influences of CFRP dimensions, load and prestress levels, and end-U-shaped wrapping reinforcement on fatigue behavior. Additionally, a fatigue life estimation model is formulated for RC beams strengthened with SB-CFRP strips. This research offers invaluable insights into the performance of fatigue-vulnerable structures employing externally bonded CFRP technology, thereby contributing to its practical application in engineering endeavors.

2. Finite element modeling

2.1. General

A three-dimensional FE model was developed using ABAQUS for predicting the fatigue responses of RC beams with externally bonded CFRP sheets. A cyclic-dependent CFRP-concrete bond-slip model was proposed and implemented into the FE model to simulate the degradation behavior of nonlinear materials. To optimize computational costs, the FE model was configured as a 1/2 model due to the beam's cross-section symmetry. The models are described in detail in the following Sections.

2.2. Fatigue model of concrete

The constitutive behavior of concrete was represented using the Concrete Damaged Plasticity (CDP) model. The axial stress-strain behavior of concrete under uniaxial compression state was simulated by the model of Kent and Park [27]. Parameters describing the concrete model, such as dilation angle, eccentricity, f_{b0}/f_{c0} ratio, K value, and viscosity, were set to 31°, 0.1, 1.16, 0.67, and 0.001, respectively [4].

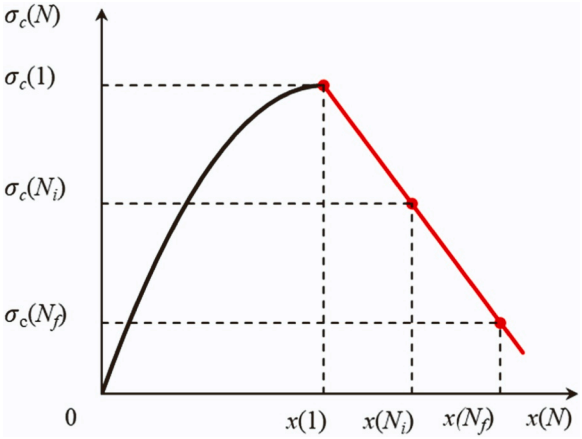

Fig. 2. The relationship between residual strength of concrete and the number of loading cycles.

In the realm of constant amplitude fatigue loading, as the number of cyclic fatigue loads increases, there is a notable rise in the accumulation of residual strain ε_{cr}, alongside a discernible decline in both the elastic modulus and strength of concrete [28,29], as shown in Fig. 1. The experimental research by Holmen [28] and Bennet and Raju [29] showed that the accumulation of internal concrete damage under repeated fatigue loading gradually reduced the elastic modulus of concrete. Drawing from the empirical findings of [28,29], EL-Tawil et al. [30] formulated an equation for determining the effective elasticity modulus of concrete E_n following a specified number of loading cycles n, presented as follows:

$$E_n = (1 - 0.33n/N_c)E_c \tag{1}$$

where $E_c = 4730\sqrt{f_c'}$ represents the Young's modulus of intact concrete [31]; N_c represents the fatigue life of concrete, denoting the number of cycles necessary for concrete to reach failure when subjected to fatigue loading [32], and can be determined as:

$$S_{ci} = \mathrm{A} + \mathrm{B}\log_{10}N_c \tag{2}$$

where $S_{ci} = \frac{\sigma_{ci}}{f_c'}$ denotes the ratio of the maximum compressive stress σ_{ci} at the n_i cycle to the uniaxial compressive strength f_c' of concrete, and A and B are constants which are taken as 0.9885 and − 0.0618, respectively [32].

Studies conducted by Hsu [33], Zanuy [34], Sima [35], Aslani [36], and Zou et al. [4,26] indicated that the degradation of concrete fatigue strength can be represented using the envelope concept of the concrete stress-strain curve, as illustrated in Fig. 2.

The residual strength of concrete at any cycle number N resembles the descending branch of the uniaxial stress-strain curve [26,38]. Zou et al. [26] linearized the descending branch, simplifying the relationship between the residual strength $\sigma_c(N)$ and the number of loading cycles N, as follows:

$$\sigma_c(N) = f_c'\{1 - Z\varepsilon_0(\log_{10}N/\log_{10}N_f)[x(N_f) - x(1)]\} \tag{3}$$

where $Z = 0.5/(\varepsilon_{50u} - \varepsilon_0)$ in which $\varepsilon_{50u} = (3 + 0.29f_c')/(145f_c' - 100)$ denotes the strain corresponding to 50 % of the compressive strength of concrete f_c', and ε_0 is the strain at f_c' [27].

2.3. Fatigue model of reinforcement

The behavior of steel reinforcements was described using the elastic-plastic constitutive model in accordance with GB50010–2010 [39].

Table 1
Stress and slip values for bond stress-slip constitutive characteristic points [39].

Characteristic points	Crack, (s_0, τ_0)	Peak value, $(s_{\max}, \tau_{\max})$	Remnant, (s_r, τ_r)
Bond stress τ (Mpa)	$\tau_0 = 2.5f_t$	$\tau_{\max} = 3f_t$	$\tau_r = f_t$
Slip s (mm)	$s_0 = 0.025d$	$s_{\max} = 0.04d$	$s_r = 0.55d$

Note: d is the diameter of the reinforcement; ft is the axial tensile strength of concrete.

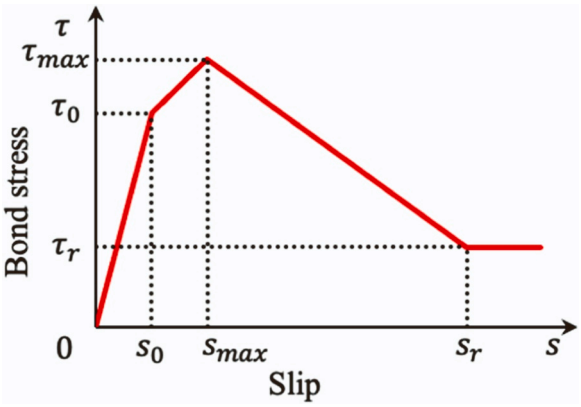

Fig. 3. Bond stress-slip constitutive relationship.

During high-cyclic fatigue loading, the predominant failure mode of steel bars in tension is characterized by brittle fracture, decreasing the effective cross-sectional area of the steel reinforcement [40]. The approach recommended by Feng et al. [40] was employed to describe the effective area of fatigued steel bars, as follows:

$$A_s^f(n) = A_s\left[1 - n/N_s\left(1 - \sigma_{s,\max}/f_y\right)\right] \tag{4}$$

where $A_s^f(n)$ represents the effective cross-sectional area; A_s denotes the initial area; $\sigma_{s,\max}$ and f_y are the peak stress under fatigue loading and the yield strength, respectively; N_s is the fatigue life of reinforcement, primarily dependent on the reinforcement stress amplitude $\Delta\sigma$, and is calculated as [41]:

$$\log_{10}N_s = 7.253 - 0.0056\Delta\sigma \tag{5}$$

With increasing fatigue loading, concrete weakens, leading to higher tensile stress in steel reinforcement. The steel's elastic modulus remains constant during this period [42]. Therefore, the Miner linear fatigue accumulation criterion was employed to determine the cumulative damage D_s of the tensioned steel bars, as follows:

$$D_s = \sum \frac{n_i}{N_s} \tag{6}$$

where n_i is the cyclic number for the specified stress amplitude of tensile steel rebars $\Delta\sigma$.

2.4. Interface between steel and concrete

The bonding between steel reinforcement and concrete interfaces significantly influences the load-carrying capacity of flexural members. The model given in GB50010–2010 [39] was used to describe the bond-slip relationship between tensioned steel bars and concrete. As shown inFig. 3 and Eq. (7) , this model consists of four parts, with the corresponding curve parameters listed in Table 1 [39].

It is noteworthy that the effect area $A_s^f(n)$ of fatigued steel bars steadily diminishes with the progression of cycle periods, as depicted in Eq. (4). Furthermore, as outlined in Eq. (7) and Table 1, the bonding slip

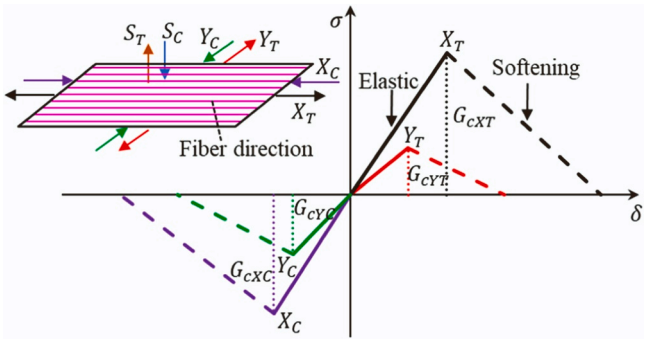

Fig. 4. Damage modeling of CFRP composites.

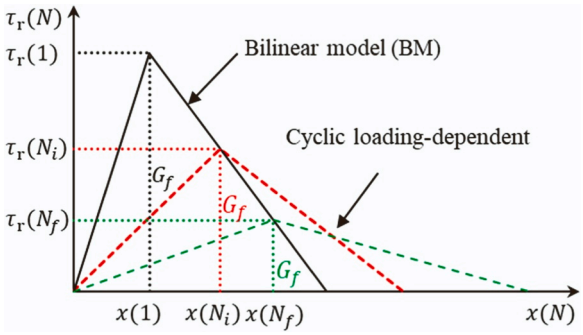

Fig. 5. Cyclic Loading-Dependent Bilinear Model (CLDBM).

s in the model relating to the interaction between concrete and reinforcement steel is a function of the diameter d of the steel reinforcements. Consequently, the decrease in the effective area $A_s^f(n)$ causes a reduction in the diameter d of the steel, thereby influencing the bonding slip dynamics between reinforcement steel and concrete.

$$\tau = \begin{cases} \dfrac{\tau_0}{s_0}s & 0 \le s \le s_0 \\ \tau_0 + \dfrac{\tau_{\max}-\tau_0}{s_{\max}-s_0}(s-s_0) & s_0 < s \le s_{\max} \\ \tau_a + \dfrac{\tau_r-\tau_{\max}}{s_r-s_{\max}}(s-s_{\max}) & s_{\max} < s \le s_r \\ f_t & s > s_r \end{cases} \tag{7}$$

2.5. CFRP

The fatigue response of CFRP composites was predicted using damage mechanics. The secondary stress-based failure model given by Hashin [43] was used to evaluate the CFRP fatigue damage. Fig. 4 illustrates the equivalent stress-displacement behavior of anisotropic CFRP under various failure modes (fiber rupture and buckling, matrix cracking, and fragmentation) represented by four bilinear elastic softening curves. The area under the curve represents the dissipative energy required for the fracture.

The stress-displacement relationships for fiber fracture and buckling/kinking are

$$d_f^t = (\frac{\sigma_{11}}{X_T})^2 + \alpha(\frac{\tau_{12}}{S_L})^2 \quad \text{for } \sigma_{11} \ge 1.0 \tag{8}$$

$$d_f^c = \left(\frac{\sigma_{11}}{X_T}\right)^2 \quad \text{for } \sigma_{11} < 1.0 \tag{9}$$

When modeling matrix cracking and crushing, the stress-strain models are expressed as

$$d_m^t = \left(\frac{\sigma_{22}}{Y_T}\right)^2 + \left(\frac{\tau_{12}}{S_L}\right)^2 \quad \text{for } \sigma_{22} \ge 1.0 \tag{10}$$

$$d_m^c = \left(\frac{\sigma_{22}}{2S_T}\right)^2 + \left[\left(\frac{Y_c}{2S_T}\right)^2 - 1\right]\frac{\sigma_{22}}{Y_c} + \left(\frac{\tau_{12}}{S_L}\right)^2 \quad \text{for } \sigma_{22} < 1.0 \tag{11}$$

where d_f^t, d_f^c and d_m^t, d_m^c represent the internal damage variables in the fiber and matrix phases under tension or compression loadings; σ_{11} and σ_{22} denote stress components of the effective stress tensor; τ_{12} represents shear in plane or axial stress; X_T and X_C stand for tensile and compressive strength in the direction of the fiber; Y_T and Y_c denote tensile and compressive strength in the direction of the matrix; S_L and S_T represent shear strength in the longitudinal and transverse directions, respectively; and α is a coefficient defining the contribution of shear stress to the fiber tensile initiation criterion and was taken as 1.

2.6. Cyclic loading-dependent interface between CFRP and concrete

Previous studies [44–47] primarily focused on the debonding issue at the CFRP-concrete interface. Four interface models are available, including bilinear [48–52], linear-parabolic [53,54], exponential and trapezoidal [50,51,55–57]. However, these models do not fully consider the influence of cyclic loading on interface debonding. Hence, adjustments are needed for the bilinear model, depicted in Fig. 5, to account for performance degradation due to periodic fatigue loading. A typical bilinear model used at the initial cycle is outlined as follows [48]:

$$\tau_r = \begin{cases} \tau_{\max}x & if(x \le 1) \\ \dfrac{\tau_{\max}(s_f/s_0 - x)}{(s_f/s_0 - 1)} & if(1 < x \le s_f/s_0) \\ 0 & if(x \ge s_f/s_0) \end{cases} \tag{12}$$

where $x = s/s_0$; s, s_0, and s_f are the macro-slips corresponding to the interfacial bond strength; and is the interfacial peak bond strength, which can be defined as follows [48]:

$$\tau_{\max} = 1.5\beta_w f_t \tag{13}$$

$$s_0 = 0.0195\beta_w f_t \tag{14}$$

$$\beta_w = \sqrt{\frac{2.25 - b_f/b_c}{1.25 + b_f/b_c}} \tag{15}$$

in which f_t is the concrete tensile strength; β_w is the CFRP's width influence factor on the concrete; b_f and b_c are CFRP's bonding width and the width of the concrete, respectively.

Experiments [25,58] showed that debonding primarily occurred within the concrete layer. Interface failure between steel and concrete results from crack propagation and concrete fatigue. Therefore, the degradation of interface stiffness is similar to that of concrete [37]. According to concrete fatigue failure criteria, fatigue failure takes place when the fatigued concrete's residual strength declines to the stress at peak fatigue load $p_{\max}$. The fatigue failure criterion for interface bond strength was assumed to be as follows:

$$\tau_r(N_f) \le \tau_{p,\max} \tag{16}$$

where $\tau_r(N_f)$ represents the residual fatigue strength of the interface; $\tau_{p,\max}$ is the interface traction force corresponding to the peak fatigue load $p_{\max}$.

Using the concrete envelope concept and Eq. (12), the relationship between the residual strength $\tau_r(N_f)$ after interfacial bond strength degradation and the number of cycles N can be further described. The relationship curve is shown in Fig. 5. By defining the relative life ratio as $r(N) = [x(N) - x(1)]/[x(N_f) - x(1)] = \log_{10}N/\log_{10}N_f$ [38], and setting

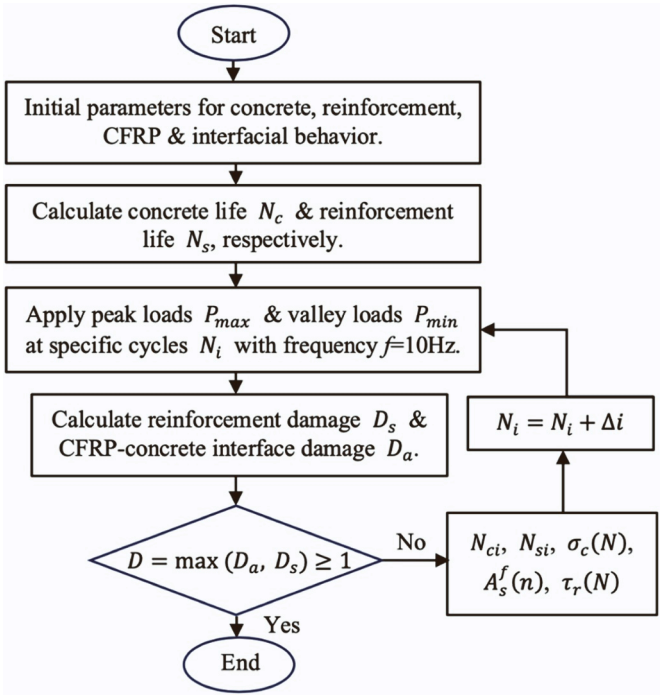

Fig. 6. FE analysis flow chart.

the boundary conditions as $\tau_r(1)|_{x(N)=x(1)} = \tau_{\max}$ and $\tau_r(N_f)|_{x(N)=x(N_f)} = \tau_{p,\max}$, the Cyclic Loading-Dependent Bilinear Model (CLDBM) can be defined as follows:

$$\tau_r(N) = \tau_{\max}\frac{s_f/s_0 - \{(\log_{10}N/\log_{10}N_f)[x(N_f)-1]+1\}}{s_f/s_0 - 1} \tag{17}$$

Cyclic loading degrades the CFRP-concrete interface strength before debonding, while the interface fracture energy G_c remains constant [59]. Hence, the interfacial bond strength at any cycle number N can be determined by substituting $\tau_r(N)$ of the CFRP-concrete interface after N cycles of loading into Eq. (12).

2.7. Failure criterion and calculation procedure

In instances where a RC beam reinforced with CFRP is subjected to high-cyclic loading, potential failure modes encompass concrete crushing within the compression zone, fracture of steel reinforcement, fracture of CFRP, or debonding at the CFRP-concrete interface [4]. Previous studies [16,60–62] have highlighted premature fatigue fracture of steel reinforcements and stripping failure at the CFRP-concrete joint interface as predominant failure mechanisms. Owing to the intricate nature of degradation-induced mechanisms, predicting the primary mode of failure presents challenges [49]. Consequently, an initial step involves quantifying the extent of CFRP-concrete debonding through the utilization of the average damage value D_a across all interface elements. Subsequently, a comparison is conducted between D_a and the cumulative damage of reinforcement D_s calculated employing Miner's criterion (Eq. (6)). Should either value reach a cumulative threshold of 1, failure occurs, as outlined below:

$$D = \max(D_a, \quad D_s) = 1 \tag{18}$$

Fig. 6 demonstrates the stepwise implementation process of the FE analysis for determining the fatigue failure mode. Fatigue loading can be categorized into two main types: constant-amplitude cyclic load and variable-amplitude cyclic load. Typically, constant amplitude testing serves as the most straightforward and often quickest method for determining the fatigue strength curves of structural elements. The

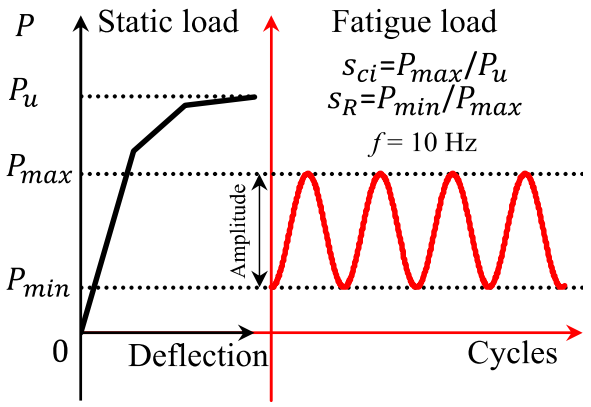

Fig. 7. Static and fatigue loading methods.

authors in [4,26] employed a comparable loading scheme, which was consistent with studies conducted by other researchers, to investigate members under uniaxial constant-amplitude tensile cycle loading [63], axial constant-amplitude cyclic compression [64,65], and constant-amplitude bending cycles [16, 38, 66]. The specimens were subjected to constant-amplitude fatigue loading. Fig. 7 illustrates configurations for both four-point bending and three-point bending loads, encompassing static and fatigue loading behaviors, in which P_u represents the ultimate load, P_{max} and P_{min} are the peak load and valley load of fatigue loading, respectively, and $S_{ci} = P_{\max}/P_u$ and $S_R = P_{min}/P_{\max}$ are the load level and stress ratio, respectively, and $\Delta P = P_{\max} - P_{\min}$ indicates the constant amplitude of fatigue loading amplitude.

The prestress on the CFRP was applied by adding an initial stress to the CFRP, which was directly proportional to the ultimate tensile strength of the CFRP [38].

2.8. Element details and interaction properties

Three-dimensional FE models developed for RC beams reinforced with both SB-CFRP and BB-CFRP sheets are presented in Fig. 8. The concrete was modeled using a simplified 3-D integrated hexahedral element with 8 nodes (C3D8R) while the steel reinforcement was modeled utilizing 3-D truss elements with 2 nodes (T3D2). For CFRP fatigue damage assessment, 3D doubly curved thin or thick shell elements with 4 nodes (S4R) were used.

The bond-slip behavior between the main reinforcement and concrete was simulated using nonlinear two-node spring elements. Concrete-CFRP contact was modeled via bond-slip relations between faces and nodes, with initial constitutive relationships specified in Eq. (12). Bonding degradation was assessed using the newly developed Cyclic Loading-Dependent Bilinear Model (CLDBM). Additionally, stirrups and ties were constrained to the concrete elements through embedded regions.

3. FE model validation

3.1. Experiments used to validate the FE model

The literature review indicates that there is a scarcity of studies focusing on experimental investigations into the fatigue response of SB-CFRP-strengthened beams. Existing literature primarily emphasizes monotonic bending tests of such strengthened beams. To validate the developed FE model, the experimental outcomes of RC beams with various configurations of CFRP sheets under both monotonic and fatigue loading conditions are compared with the predicted numerical results. The geometric and material properties of the tested specimens, delineated in Fig. 9 and Table 2, respectively, are categorized into nine groups based on their strengthening and loading methodologies.

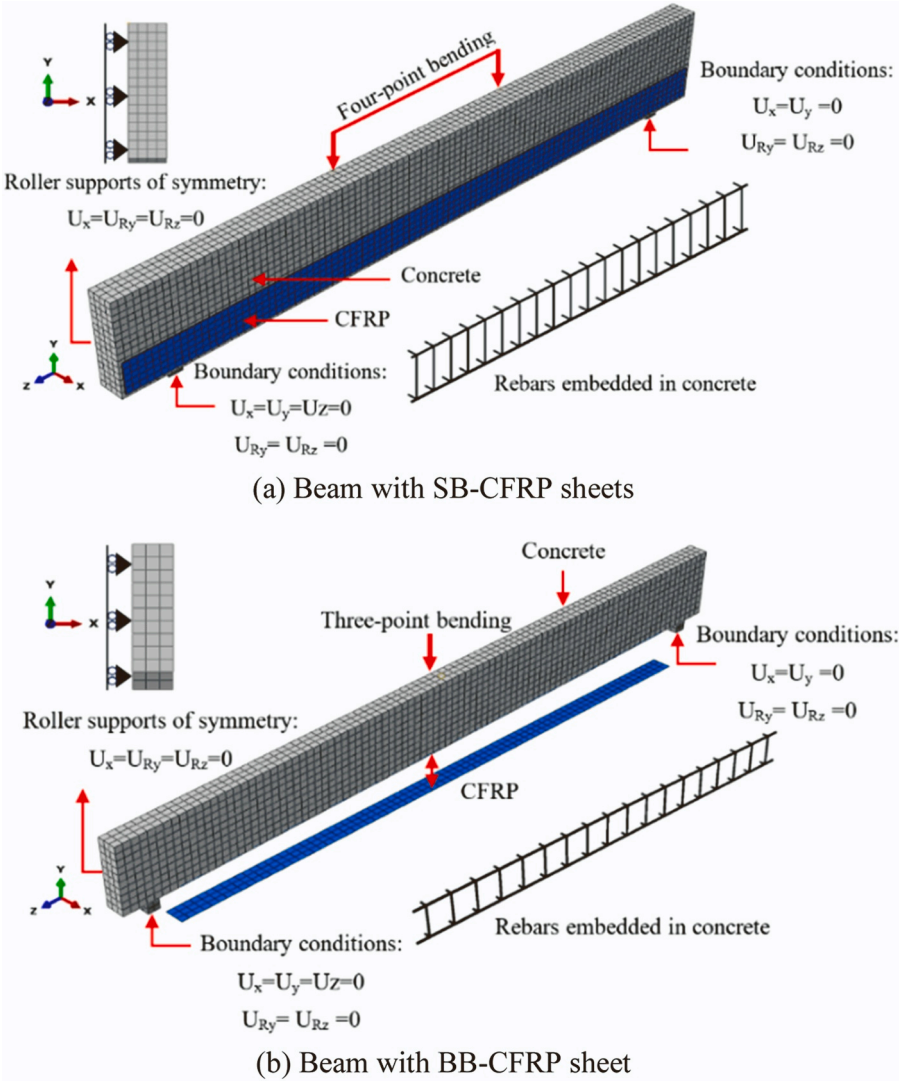

Fig. 8. Meshing configurations and boundary conditions.

Group 1 (G-1) specimens entail RC beams strengthened with SB-CFRP sheets under four-point bending, employing CFRP sheets of 1.02-mm thick and two distinct widths of 50 mm and 100 mm for the external reinforcement of RC beam specimens S50 and S100, respectively (see Fig. 9(a)) [21,23]. In Group 2 (G-2) specimens, BB-CFRP sheets with pre-stressing levels of 5 % and 11 % are utilized for reinforcing RC beam specimens P5 and P11, as demonstrated in Fig. 9(b) and elaborated in Table 2 [67]. Group 3 (G-3) specimens encompass RC beam specimens UW1, UW2, and UW3, strengthened with U-shaped wrapping CFRP sheets featuring widths of 200 mm and 400 mm, as depicted in Fig. 9(c) and Table 2 [68]. Similarly, Group 4 (G-4) specimens comprise RC beam specimens 1 L, 2 L, and 3 L, reinforced with BB-CFRP sheets of 1, 2, and 3 layers, respectively, as depicted in Fig. 9 (d) and detailed in Table 2 [69]. In Group 5 (G-5), RC beam specimens L520, L1040, and L1560 were reinforced with BB-CFRP sheets of varying lengths: 520 mm, 1040 mm, and 1560 mm, respectively, as illustrated in Fig. 9(e) and shown in Table 2 [70]. Group 6 (G-6) specimens involve RC beam specimens 2D16, 5D10, and 2D28, strengthened with BB-CFRP sheets featuring three different longitudinal steel bar configurations: 2ϕ16, 5ϕ10, and 2ϕ28, as presented in Fig. 9(f) and Table 2 [71]. All specimens were subjected to a monotonic loading scheme. Further particulars concerning the experimental specimens are available in references [21,23,67–71].

Huang [72] conducted three-point tests on the static and fatigue behavior of RC beams strengthened with BB-CFRP strips in 1560-mm long, 100-mm width, and 0.23-mm thick, as shown in Table 2, Group 7 (G-7) The tested beams had the same dimensions of G-2 specimens shown in Fig. 9(b). One beam was under static loading while two beams were subjected to constant amplitude load in fatigue loading with frequency f= 10 Hz [16].

Furthermore, as displayed in Table 2, Group 8 (G-8) specimens encompass two RC beam specimens, namely B100P10 %-27.5 and B100P10 %-30, reinforced with BB-CFRP strips at a prestress level of 10% under cyclic fatigue loading at 27.5 kN and 30 kN, respectively, as reported by Xie [73]. These tested specimens maintain identical geometric dimensions to B100, including the dimensions of steel bars, CFRP, and reinforced beams illustrated in Fig. 9(b), albeit with distinct material properties, as indicated in Table 2.

Group 9 (G-9) comprises specimens tested by Huang [74] with geometric dimensions mirroring those of B100 (G-7), as shown in Fig. 9 (g). However, a distinctive feature of G-9 is the incorporation of a U-shaped reinforcement configuration. The experimental setup involved reinforcing RC beams with CFRP at a prestress level of 22 %, subsequently subjecting them to fatigue cyclic loading at 37.5 kN and 40 kN. FE analysis was then conducted under loading levels of Sci = 0.58 and 0.62, corresponding to peak loads of P_u = 65 kN, with load magnitudes of 37.5 kN and 40 kN, respectively.

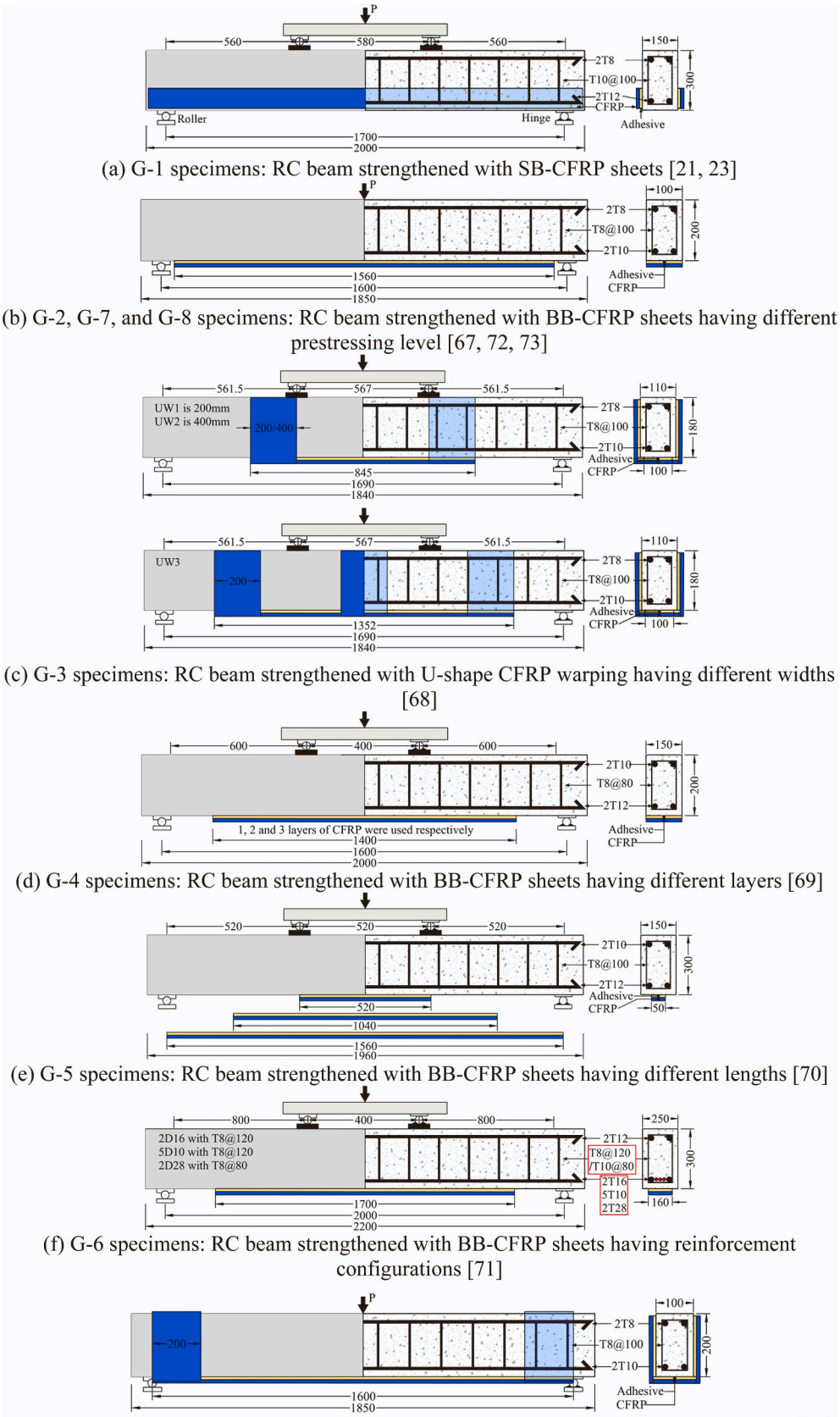

Fig. 9. Test setup, reinforcement and CFRF details, and cross-section of the beams.

Table 2
Material properties of tested specimens.

Group	Loading scheme	Specimen	f_c (MPa)	f_y (MPa)	f_u (MPa)	E_s (GPa)	f_{CFRP} (MPa)	E_{CFRP} (GPa)	Ref.
G-1	Monotonic	S100	50	551.5	640.2	199.9	1240	73.77	[21,23]
		S50	50	551.5	640.2	199.9	1240	73.77	
G-2		P11 %	37.3	328	452	226	2971	240	[67]
		P5 %	37.3	328	452	226	2971	240	
G-3		UW1	54	611	-	202	2500	215	[68]
		UW2	54	611	-	202	2500	215	
		UW3	54	611	-	202	2500	215	
G-4		1 L	25.2	400	578	206	2845	237	[69]
		2 L	25.2	400	578	206	2845	237	
		3 L	25.2	400	578	206	2845	237	
G-5		L1560	29	495	760	207	2640	165	[70]
		L1040	29	495	760	207	2640	165	
		L520	29	495	760	207	2640	165	
G-6		2D16	25	453	711	209	4950	240	[71]
		5D10	25	462	622	190	4950	240	
		2D28	25	379	602	203	4950	240	
G-7		B100	25	400	-	206	4750	230	[72]
	Fatigue	B100-27.5	25	400	-	206	4750	230	
		B100-30	25	400	-	206	4750	230	
G-8		B100P10 %-27.5	37.3	307	452	206	2830	240	[73]
		B100P10 %-30	37.3	307	452	206	2830	240	
G-9		B100P22 %U-37.5	31	344	520	226	2971	230	[74]
		B100P22 %U-40	31	344	520	226	2971	230	

Table 3
Comparison between the FE and experimental results of RC beams under monotonic loading.

Group	Specimen	$P_{u,exp}$ (kN)	$P_{u,FE}$ (kN)	$\Delta_{u,exp}$ (mm)	$\Delta_{u,FE}$ (mm)	$P_{u,FE}/P_{u,exp}$	$\Delta_{u,FE}/\Delta_{u,exp}$	Ref.
G-1	S100	194.56	188.44	13.70	13.43	0.97	0.98	[21,23]
	S50	163.59	168.07	13.40	13.71	1.03	1.02	
G-2	P11 %	52.20	52.09	14.40	15.26	1.00	1.06	[67]
	P5 %	45.00	46.15	12.50	12.50	1.03	1.00	
G-3	UW1	59.56	59.11	18.17	18.44	0.99	1.01	[68]
	UW2	58.88	60.47	23.48	23.82	1.03	1.01	
	UW3	67.69	63.82	12.79	13.85	0.94	1.08	
G-4	1 L	61.45	61.21	10.20	10.42	1.00	1.02	[69]
	2 L	70.94	72.36	9.14	9.23	1.02	1.01	
	3 L	74.44	75.94	11.60	10.47	1.02	0.90	
G-5	L1560	166.00	165.13	6.04	6.23	0.99	1.03	[70]
	L1040	142.00	145.25	5.68	5.63	1.02	0.99	
	L520	128.00	125.66	5.50	5.66	0.98	1.03	
G-6	2D16	148.00	147.41	12.70	12.68	1.00	1.00	[71]
	5D10	179.00	177.77	15.90	16.58	0.99	1.04	
	2D28	309.00	312.00	20.10	20.42	1.01	1.02	
G-7	B100	43.70	45.03	14.59	15.00	1.03	1.03	[72]
Mean						1.0027	1.0145	
Standard deviation (SD)						0.0239	0.0379	
Coefficient of variation (CoV)						0.0238	0.0374	

3.2. Static response

Table 3 presents a comparison of the predicted ultimate load ($P_{u,FE}$) and mid-span deflection values ($\Delta_{u,FE}$) with their experimental counterparts ($P_{u,exp}$ and $\Delta_{u,exp}$) for both SB-CFRP and BB-CFRP strengthened beams under monotonic loading conditions (G-1 to G-7 specimens). The mean $P_{u,FE}/P_{u,exp}$ ratio was calculated to be 1.0027, accompanied by a coefficient of variation (CoV) of 0.0238. Furthermore, the $\Delta_{u,FE}/\Delta_{u,exp}$ ratio stands at 1.0145, with a corresponding CoV of 0.0374.

In Fig. 10, the experimental load-deflection results from monotonic bending tests are compared with the predicted numerical outcomes for G-1 to G-7 specimens. Notably, the curves forecasted by the FE simulation closely mirror the experimental data across various stages of static loading. These findings underscore the model's efficacy in accurately capturing the static response of RC beams externally reinforced with CFRP sheets.

3.3. Fatigue response

Fig. 11 presents a comparison between the predicted and experimental midspan deflection-relative life (N/N_f) curves for G-7 specimens under two load levels of S_{ci}= 0.61 and S_{ci}= 0.66 corresponding to peak loads of P_{max}= 27.5 kN and P_{max} = 30 kN, G-8 specimens under load levels of S_{ci} = 0.60 and S_{ci} = 0.65, also corresponding to peak loads of P_{max} = 27.5 kN and P_{max} = 30 kN, and finally for G-9 specimens under two load levels of S_{ci}= 0.58 and S_{ci}= 0.62 corresponding to peak loads of P_{max}= 37.5 kN and P_{max} = 40 kN.

The curves exhibit a consistent three-stage pattern: initiation, stable, and failure phases. Notably, the initiation and failure phases are relatively brief, with the stable stage constituting over 90 % of the entire fatigue life. The results indicate that higher peak loads result in greater midspan deflection of the beams. Furthermore, an increase in loading cycles (N/N_f) leads to heightened midspan deflection, contributing to a reduction in flexural stiffness due to concrete, steel reinforcement, and CFRP-concrete interface deterioration. Specifically, during the initiation stage, a significant increase in midspan deflection corresponds to rapid

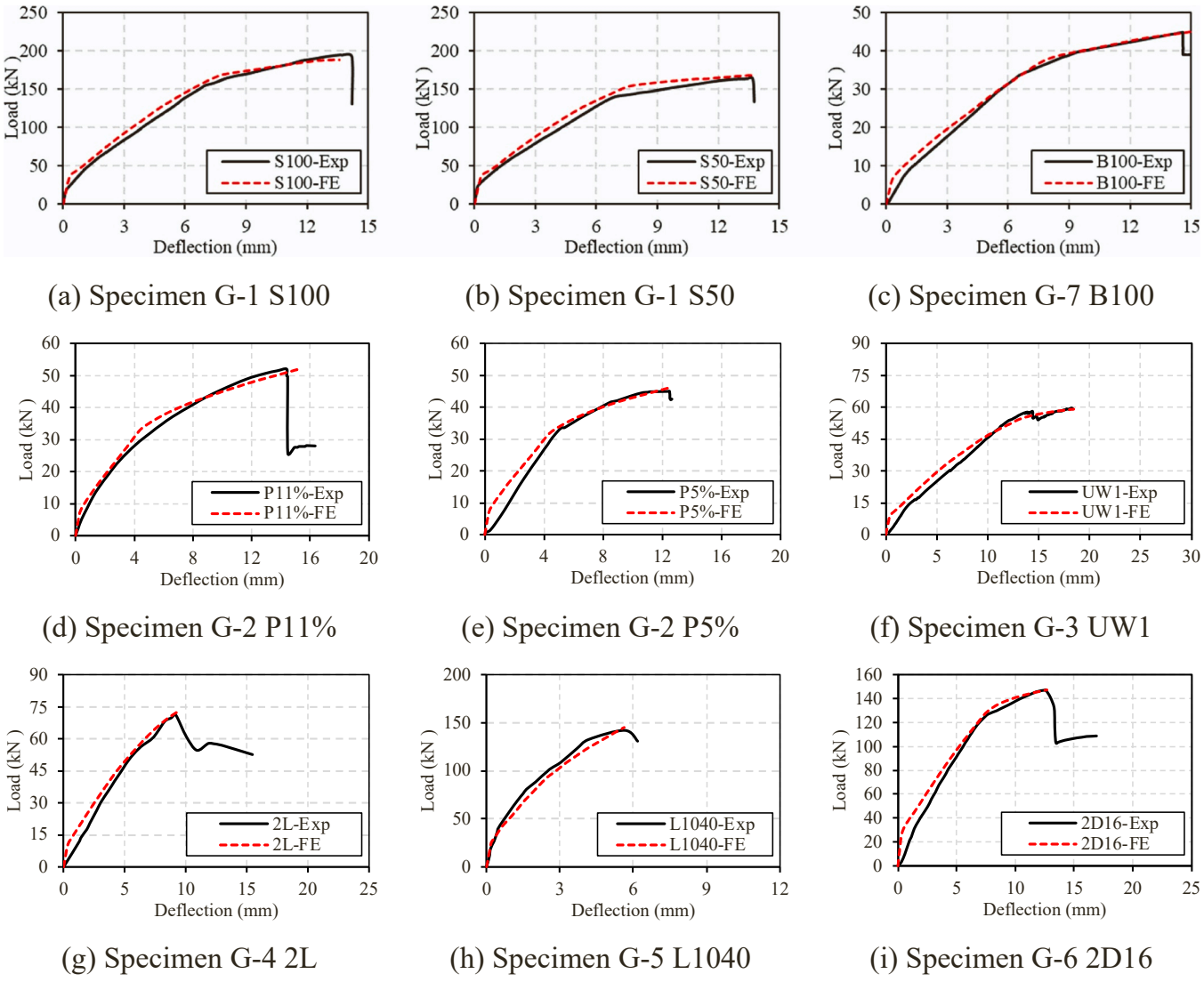

Fig. 10. Comparison of numerical and experimental load-deflection curves under static load.

fatigue flexural stiffness reduction, indicating crack initiation and propagation in the strengthened beams. In the stable stage, fatigue flexural stiffness experiences steady growth, reflecting slower crack propagation. However, during the failure phase, fatigue flexural stiffness diminishes rapidly, corresponding to steel reinforcement yielding and rupturing, as well as CFRP-concrete interface debonding.

Table 4 provides a comparison of midspan deflection between experimental outcomes and FE analysis results at 10 %, 20 %, 40 %, 60 %, 80 %, 90 %, and 100 % of relative life N/N_f. Analysis of the data reveals that an augmentation in N/N_f correlates with an increase in midspan deflection of the beam. Notably, the comparison highlights that for identical load levels S_{ci}, the midspan deflection of RC beams reinforced with prestressed CFRP sheets is lower compared to those reinforced with non-prestressed CFRP sheets. However, it is observed that the efficacy of prestressing in mitigating midspan deflection diminishes with an escalation in the N/N_f ratio. This trend aligns with findings presented by the authors concerning the effectiveness of prestressed externally bonded CFRP sheets in reinforcing RC slabs subjected to fatigue loading [4].

Overall, the experimental and predicted midspan deflection- N/N_f curves illustrated in Fig. 11 and Table 4 demonstrate satisfactory alignment. Notably, the average error remains below ± 10 %. These findings suggest that the developed Cyclic Loading-Dependent Bilinear Model (CLDBM) adeptly captures the fatigue degradation traits of CFRP-reinforced beams. As a result, the established FE model proves its validity in accurately predicting the fatigue behavior of RC beams strengthened with externally bonded CFRP systems.

Fig. 12 illustrates the comparison between the observed failure modes in experimental [74] and numerical analyses of steel reinforcements and CFRP sheets in an RC beam specimen labeled B100P22 %U-40, which was strengthened with BB-CFRP sheets at a prestress level of 22 % and U-shaped CFRPs at the beam's ends. In the FE analysis, it was noted that under cyclic fatigue loading, the tensile reinforcement bars situated at the midspan of the beam experienced a progression to their yield strength and subsequent damage due to the accumulation of fatigue. This process is depicted in Fig. 12(a). Consequently, there was a sudden surge in tensile stresses within the BB-CFRP sheet, leading to their detachment from the beam ends. However, it is noteworthy that there was no observed detachment of the U-shaped CFRPs during the experiments, as illustrated in Fig. 12(b). A comparison of the experimental and numerical failure modes shows that the developed model is able to replicate the failure modes observed in RC beams strengthened with prestressed BB-CFRP sheets and U-shaped CFRPs at the beam's ends with a reasonable level of accuracy.

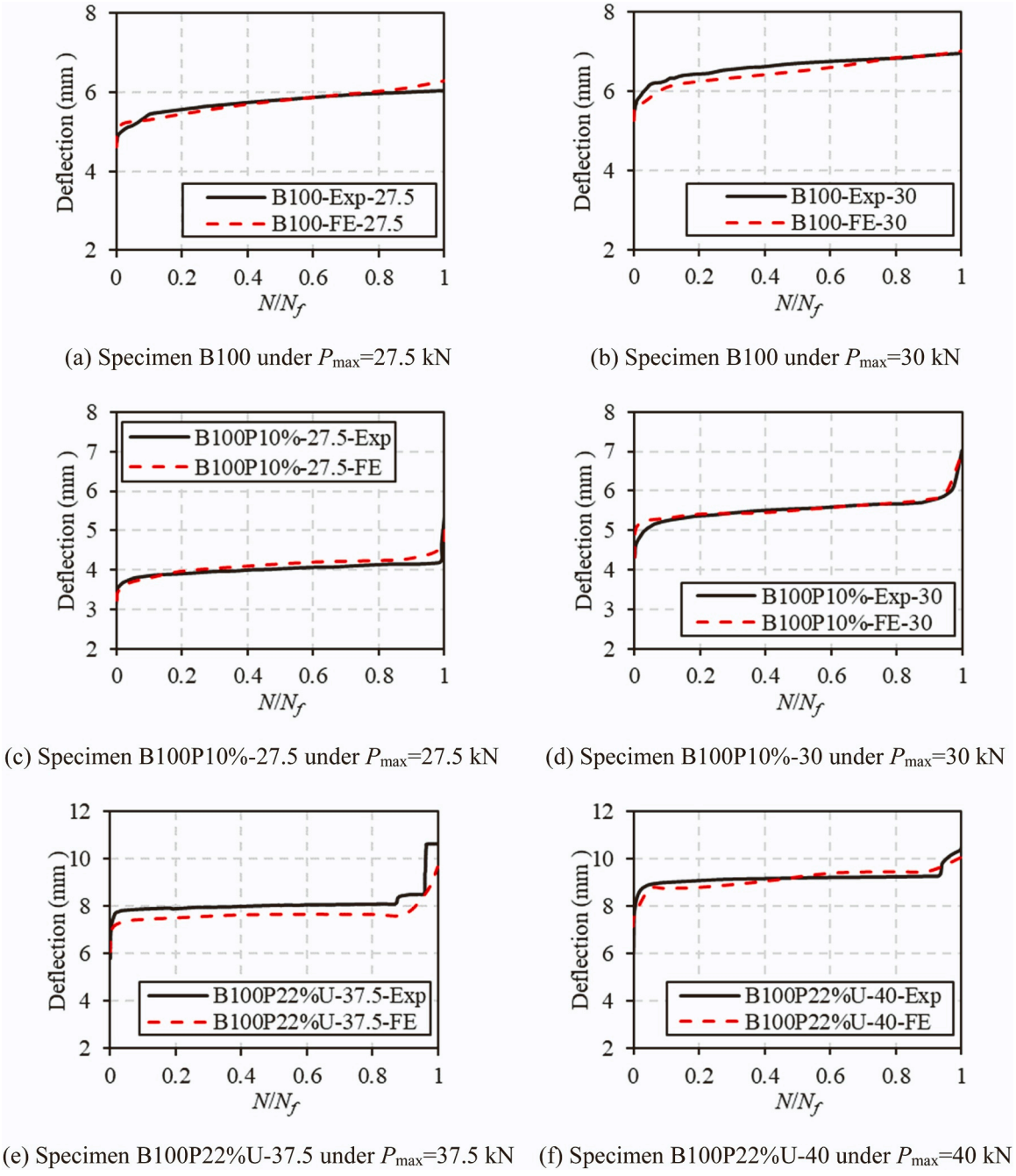

(a) Specimen B100 under P_{max}=27.5 kN (b) Specimen B100 under P_{max}=30 kN

(c) Specimen B100P10%-27.5 under P_{max}=27.5 kN (d) Specimen B100P10%-30 under P_{max}=30 kN

(e) Specimen B100P22%U-37.5 under P_{max}=37.5 kN (f) Specimen B100P22%U-40 under P_{max}=40 kN

Fig. 11. Comparison of numerical and experimental deflection-relative life curves.

4. Parametric studies

Parametric studies were conducted using the validated FE model to explore the fatigue response of SB-CFRP-reinforced beams, considering factors including CFRP dimensions, loading level S_{ci}, prestressing level, and the presence of U-shaped wrapping at beam ends. The fatigue loading conditions, characterized by the stress ratio (S_R) and frequency (f) of constant amplitude load, were set at 0.3 and 10 Hz, respectively, in alignment with previous studies [2,8,16,72,74–77].

It is noteworthy that, in compliance with ACI 215R-74 [78], the fatigue threshold is defined as the load corresponding to 2×10^6 cycles. When a reinforced beam endures this cycle count without failure, it is considered to possess an infinite fatigue life [16,79]. However, discerning a distinct failure pattern for specimens exhibiting infinite fatigue life in experimental settings presents challenges. In numerous fatigue assessments conducted on CFRP-reinforced beams [2,8,16,75,76], the cycle counts typically fall below 2×10^6, often significantly lower. For instance, fatigue tests conducted by Wang et al. [16] on three sets of CFRP-reinforced beams subjected to varying load levels resulted in average fatigue life values of 9.5×10^5 cycles, 6.5×10^5 cycles, and 5×10^5 cycles, respectively. Similarly, Guo [75] and Li [8] reported fatigue life outcomes for different sets of CFRP-reinforced beams, with fatigue life values ranging from 3.5×10^5 cycles to 8.3×10^5 cycles, contingent upon the applied load levels. Therefore, to ensure effective replication of tests in FE analysis and to discern clear trends, the study aligns the number of test cycles with the observed range in experimental studies [2,8,16,75,76].

Table 4
Comparison between the FE and experimental results of RC beams under fatigue loading.

Group	Specimen	N/N_f	$\Delta_{u,FE}$ (mm)	$\Delta_{u,exp}$ (mm)	$\Delta_{u,FE}/\Delta_{u,exp}$	Ref.
G-7	B100-27.5	0.1	5.30	5.45	0.97	[72]
		0.2	5.45	5.56	0.98	
		0.4	5.70	5.75	0.99	
		0.6	5.87	5.88	1.00	
		0.8	6.08	5.98	1.02	
		0.9	6.22	6.01	1.03	
		1	6.38	6.05	1.05	
	B100-30	0.1	5.90	6.33	0.93	
		0.2	6.04	6.46	0.93	
		0.4	6.25	6.64	0.94	
		0.6	6.52	6.76	0.96	
		0.8	6.85	6.85	1.00	
		0.9	6.90	6.92	1.00	
		1	7.02	6.97	1.01	
G-8	B100P10 %-27.5	0.1	3.77	3.71	1.02	[73]
		0.2	3.97	3.76	1.06	
		0.4	4.13	3.85	1.07	
		0.6	4.25	3.92	1.08	
		0.8	4.40	3.99	1.10	
		0.9	4.43	4.01	1.10	
		1	5.28	5.40	0.98	
	B100P10 %-30	0.1	5.31	5.25	1.01	
		0.2	5.42	5.37	1.01	
		0.4	5.46	5.51	0.99	
		0.6	5.59	5.59	1.00	
		0.8	5.70	5.67	1.01	
		0.9	5.80	5.75	1.01	
		1	6.96	7.02	0.99	
G-9	B100P22 %U-37.5	0.1	7.45	7.88	0.95	[74]
		0.2	7.52	7.90	0.95	
		0.4	7.65	7.99	0.96	
		0.6	7.67	8.05	0.95	
		0.8	7.66	8.09	0.95	
		0.9	7.68	8.45	0.91	
	B100P22 %U-40	1	9.68	10.64	0.91	
		0.1	8.77	8.99	0.98	
		0.2	8.81	9.07	0.97	
		0.4	9.07	9.15	0.99	
		0.6	9.41	9.20	1.02	
		0.8	9.47	9.22	1.03	
		0.9	9.50	9.24	1.03	
		1	10.09	10.61	0.95	

4.1. The influences of CFRP width and load level

Four distinct widths of CFRP of 30 mm, 50 mm, 100 mm, and 150 mm were employed to evaluate the effects of the CFRP width on the fatigue response of RC beams. All specimens were subjected to a consistent peak load of $P_{max} = 113$ kN and a stress ratio of $S_R = 0.3$. The varying CFRP widths resulted in different ultimate loads P_u for each specimen, leading to disparate load levels $S_{ci} = P_{max}/P_u$ of 0.71, 0.67, 0.6, and 0.56, respectively. Further analysis delved into the impact of peak load P_{max} on the fatigue response of specimens by applying varied peak loads of 113 kN, 122.5 kN, and 132 kN, corresponding to distinct S_{ci} values of 0.6, 0.65, and 0.7, respectively, on a specimen strengthened with CFRP having a consistent width of 100 mm and a stress ratio S_R of 0.3.

Fig. 13 shows deflection vs. load cyclic curves for RC beams reinforced with different CFRP widths under varied load levels. In Fig. 13(a), beams with CFRP widths of 30 mm, 50 mm, 100 mm, and 150 mm exhibit decreasing deflection trends over identical fatigue cycles at the same peak loads. Notably, at $N = 5 \times 10^4$ and $N = 1 \times 10^5$ cycles, increasing the width from 50 mm to 100 mm results in deflection reductions of 15.5 % and 20.3 %, respectively. However, a subsequent 50 % increase to 150 mm yields only 5.5 % and 5.9 % reductions in deflection compared to the 100 mm width, respectively. Moreover, the fatigue life of the 100-mm CFRP-reinforced beam experiences a 179.9 % increase compared to the beam with a 50-mm CFRP strip, while the 150-mm width demonstrates only a 20 % increase over 100 mm. These findings imply that increasing CFRP width effectively diminishes fatigue deflection and enhances fatigue life; nevertheless, the extent of these benefits declines as the CFRP width approaches the neutral axis of the beams.

Additionally, Fig. 13(b) indicates that under the same number of cycles, beams with the same CFRP width (100 mm) show a significant increase in deflection at load levels 0.65 and 0.7 compared to the one with 0.6 ratio, highlighting the substantial impact of load levels on fatigue deflection.

Fig. 14 depicts stress and cumulative damage evolution in the main reinforcement of beams having different CFRP widths and load levels across fatigue cycles. In Fig. 14(a), the stress experienced by the main reinforcement in beams featuring different widths of CFRP follows a similar pattern when subjected to comparable fatigue loads, characterized by an initial rapid increase followed by a more gradual ascent. Specifically, the stress on the reinforcement experiences a swift escalation during the initial cycle, aligning closely with the evolution of midspan deflection, as depicted in Fig. 13(a). This correlation in stress behavior with respect to loading cycles mirrors findings from prior investigations into RC beams reinforced with BB-CFRP sheets [16,80], where the steel stress experiences a sharp surge at first, followed by a more gradual, almost linear increase. Notably, as illustrated in Fig. 14 (a), broader CFRP widths correspond to main reinforcement stress levels approaching the yield load at the point of fatigue failure.

As shown in Fig. 14(b), the total damage rate for main reinforcement in beams with CFRP strips of 30 mm and 50 mm is higher than that in beams with CFRP widths of 100 mm and 150 mm. This suggests that increasing the CFRP width positively reduces cumulative damage in the main reinforcement, significantly prolonging the beams' service life.

The fatigue stress of CFRP in reinforced beams is shown in Fig. 15(a). At the same fatigue cycle, CFRP stress decreases with increasing the CFRP width. For instance, at $N = 1 \times 10^4$ cycles, CFRP stress reduces by 13.0 %, 13.4 %, and 4.1 % for widths of 30 mm, 50 mm, and 150 mm, respectively. However, it should be noted that at these cycles, the ratio of CFRP stress to yield strength ρ_{CFRP} ranges from 23.6 % to 17.1 % for widths of 30 mm and 150 mm. Even at the fatigue failure cycle N_f, ρ_{CFRP} remains between 22.5 % and 25.7 %, indicating that CFRP stress operates at a relatively low utilization level. In contrast, the stress ratio ρ_s for steel exceeds 62.2 % at $N = 1 \times 10^4$ cycles and rises above 84.8 % at the fatigue failure cycle N_f, indicating a higher stress level for steel. Thus, CFRP fatigue stress is less affected by width compared to steel in this context.

Fig. 15(b) demonstrates the CFRP-concrete interface damage evolution for different CFRP widths and loads. The beams with CFRP strip widths of 30 mm and 50 mm experience over 70 % of their fatigue life with interface damage above 0.5; however, beams with 100-mm and wider CFRP strips exhibit lower damage, staying below 0.5. At fatigue failure, the beam strengthened with CFRP strips of 100-mm width has an interface damage of 0.44, 17% higher than the beam bonded with CFRP strip of 150-mm width, indicating that increasing CFRP width significantly reduces damage between CFRP and concrete.

It can be seen from Figs. 14(b) and 15(b) at a high load level of $S_{ci} = 0.71$ that the CFRP strip of 30-mm width experiences greater interface damage upon fatigue failure than steel. At this point, the CFRP stress suddenly drops, and steel has not yielded, indicating that the concrete crushes due to CFRP-concrete interface debonding. At $S_{ci} = 0.67$ with a 50-mm CFRP width, steel damage aligns with CFRP-concrete interface damage, leading to the same failure mode as the beam with CFRP strip width of 30 mm. The cumulative steel damage at 1 in the beam strengthened with CFRP strip of 100-mm width indicates a prominent steel rupture surpassing CFRP-concrete interface damage. The results underscore the significant influence of CFRP width and load level on failure modes in SB-CFRP-reinforced beams.

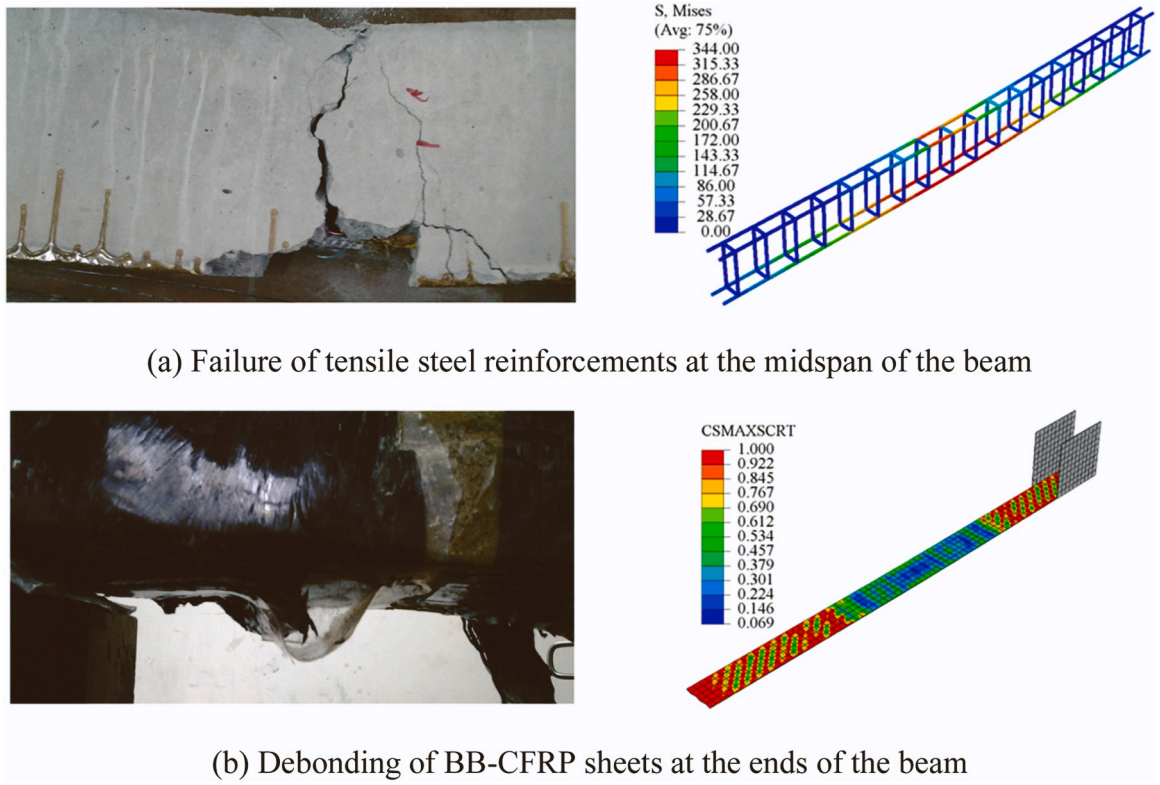

Fig. 12. Comparison of numerical and experimental failure modes of strengthened RC beams [74].

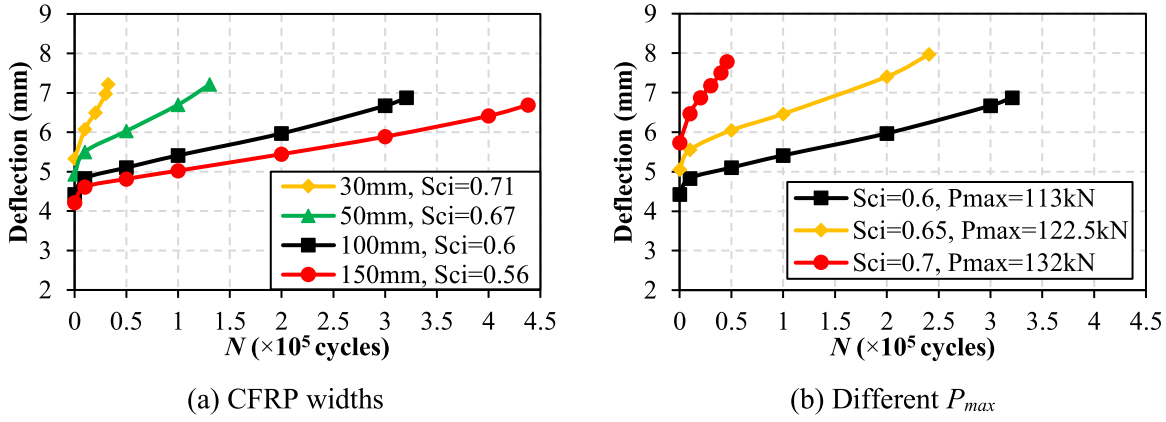

Fig. 13. The deflection-load cyclic curves of specimens with different CFRP widths and P_{max}.

4.2. *The influence of prestressing and U-shaped wrapping*

The effects of prestressing and U-shaped wrapping on the fatigue behavior of SB-CFRP strengthened beams were examined to address a gap in previous studies [21–24]. RC beams with 100-mm width CFRP strips were analyzed with the prestress levels of 0 %, 10 %, 15 %, 17 %, and 18 %. Fig. 16 illustrates the intricate relationship between deflection, steel stress, cumulative damage, CFRP stress, CFRP-concrete interface damage, and fatigue cycles.

As demonstrated in Fig. 16(a), at prestress levels of 10 %, 15 %, and 17 %, strengthened beams consistently show a two-stage deflection pattern: an initial rapid increase followed by a slower rise until failure. However, with 18 % prestress in CFRP, there is an additional rapid increase in deflection in later fatigue stages, resulting in a distinct three-stage failure. Notably, in mid and late fatigue stages (e.g., at $N = 1 \times 10^5$ and $N = 3 \times 10^5$ cycles), the prestress of 10 % in CFRP strips reduces the deflection by 26 % and 30.7 %, respectively, compared to non-prestressed case. This reduction becomes more significant with higher prestress levels, indicating that applying prestress significantly influences strengthened beams' fatigue deflection. Prestressing proves effective in reducing the deflection of RC beams under fatigue loading.

It can be observed from Fig. 16(b) that the main reinforcement stress evolution mirrors the deflection pattern in Fig. 16(a). At 18 % prestress, the stress sharply rises in the third stage, peaking at 591.9 MPa, nearing but not exceeding the tensile strength. Fig. 16(c) shows that at the $N = 1$ cycle, the CFRP stress in beams with 10 % to 18 % prestress significantly increases by 27.6 % to 43.8 % compared to the non-prestressed beam. The CFRP stress ratio ρ_{CFRP} ranges from 24.3 % to 31.3 %, showcasing the prestress advantage in maximizing CFRP strength utilization. However, the beam with 18 % prestress in CFRP strips exhibits a sudden drop in CFRP stress in late fatigue stages, indicating extensive debonding and severe failure, as demonstrated in Fig. 17.

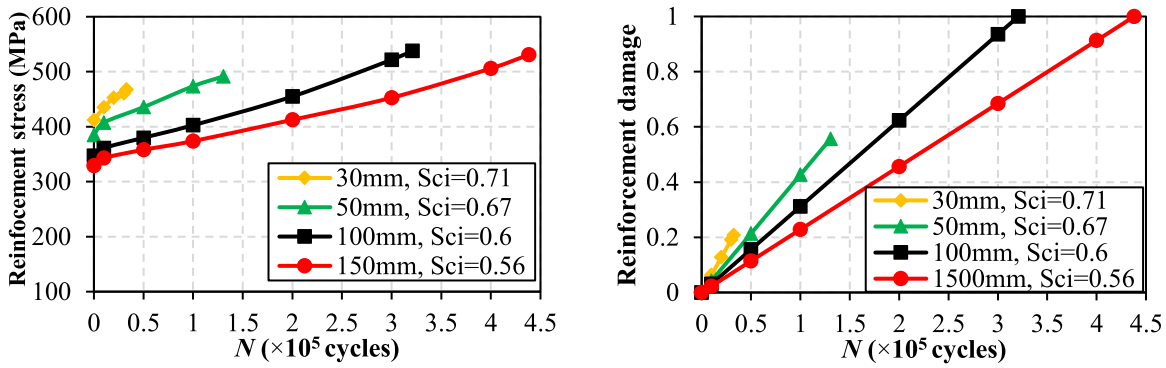

(a) Reinforcement stress vs. load cycle (b) Reinforcement damage vs. load cycle

Fig. 14. Influence of CFRP widths and load levels on the stress and damage of main reinforcement.

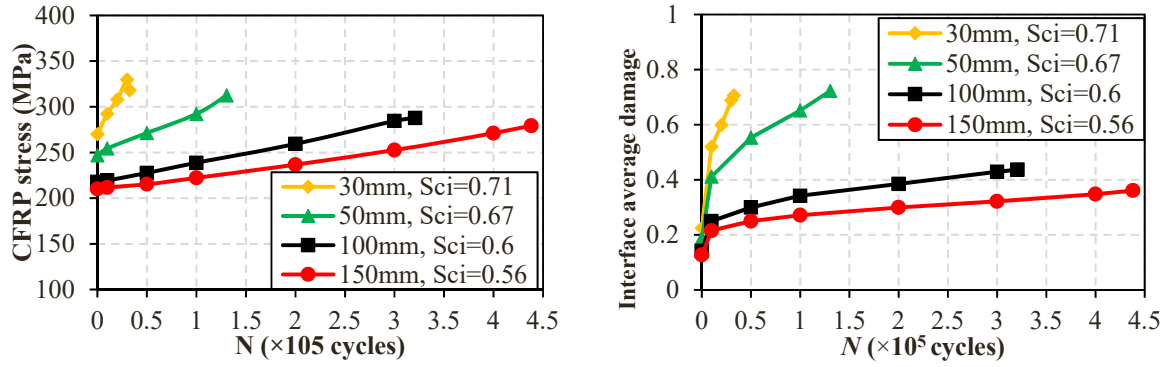

(a) CFRP stress vs. load cycle (b) Interface average damage vs. load cycle

Fig. 15. The evolution of CFRP stress and CFRP-concrete interface average damage.

Fig. 16(d) shows that the main reinforcement damage linearly increases with fatigue cycles at different prestress levels. The higher the prestress level, the slower the damage accumulation. At $N = 3 \times 10^5$ cycles, the beams with 10 % to 18 % prestress on CFRP strips show 32.9 % to 53.2 % less damage than the non-prestressed beam, Comparing Figs. 16(d) and (e), as the main reinforcement cumulative damage reaches 1, the non-prestressed beam maintains CFRP-concrete interface damage below 0.5 at $S_{ci} = 0.6$. This indicates that the primary failure mode is the main reinforcement rupture causing CFRP-concrete interface debonding. At 10 % prestress, however, the main reinforcement damage surpasses the interface damage, but there is potential for increasing CFRP stress (Fig. 16(c)). With 15 % prestress, interface damage rises, shifting from the main reinforcement rupture to CFRP-concrete interface debonding. Increasing prestress to 18 % leads to continuous main reinforcement damage escalation, but interface damage rapidly surges, suggesting substantial interface bonding deterioration, as shown in Fig. 17. Under fatigue loads, non-prestressed and low-prestress CFRP-strengthened beams mainly fail due to steel reinforcement rupture, but high prestress increases the likelihood of CFRP-concrete interface debonding. High prestress significantly and adversely affects the bonding behavior of the CFRP-concrete interface in beams strengthened with CFRP sheets. This highlights the intricate relationship between prestress levels and failure mechanisms.

Applying prestress to CFRP allows it to reach its full-strength potential, but this method has difficulties in practice. To address issues, U-shaped stirrups as illustrated in Fig. 18 were used at the beam ends [38,76,81]. This addition enabled a deeper exploration of dual failure modes: CFRP-concrete interface damage and cumulative steel reinforcement damage. Fig. 19 presents a comparative evaluation of steel reinforcement cumulative damage and average damage to the CFRP-concrete interface for two sets of strengthened beams, with prestress levels at 0 %, 10 %, and 18 %.

As shown in Fig. 19(a), the use of U-shaped wrapping of CFRP strips at the ends of the beams with prestress leads to a continuous reduction in average damage to the CFRP-concrete interface throughout their service life. This reduction becomes more significant with additional fatigue cycles, reaching 14.04 % and 30.83 % reductions at N_f, respectively. The use of U-shaped wrapping substantially mitigates the average damage to the CFRP-concrete interface caused by high prestress.

U-shaped wrapping delays damage accumulation in the main reinforcement, extending the fatigue life of strengthened beams as indicated in Fig. 19(b). This underscores the efficacy of U-shaped wrapping in enhancing the durability and performance of CFRP-strengthened beams. The research findings highlight its potential as a viable design solution for optimizing structural integrity and extending the lifespan of these reinforced concrete structures. Fig. 20 presents the numerical simulation results on the interface damage of SB-CFRP-strengthened beams with U-shaped wrapping.

4.3. *Vibration detection analysis of CFRP fatigue delamination*

Fig. 21 presents the correlation between the frequency, displacement, and fatigue cycle of specimens. Under fatigue loading, two distinct peaks in vibration displacement emerge at the midspan: the first peak in the red region and the second peak in the light blue region, serving as indicators of fatigue damage. Up to $N = 7 \times 10^5$ cycles, both peaks display stable growth, signifying consistent monitoring of accumulated damage. At this point, the average damage to the CFRP-concrete

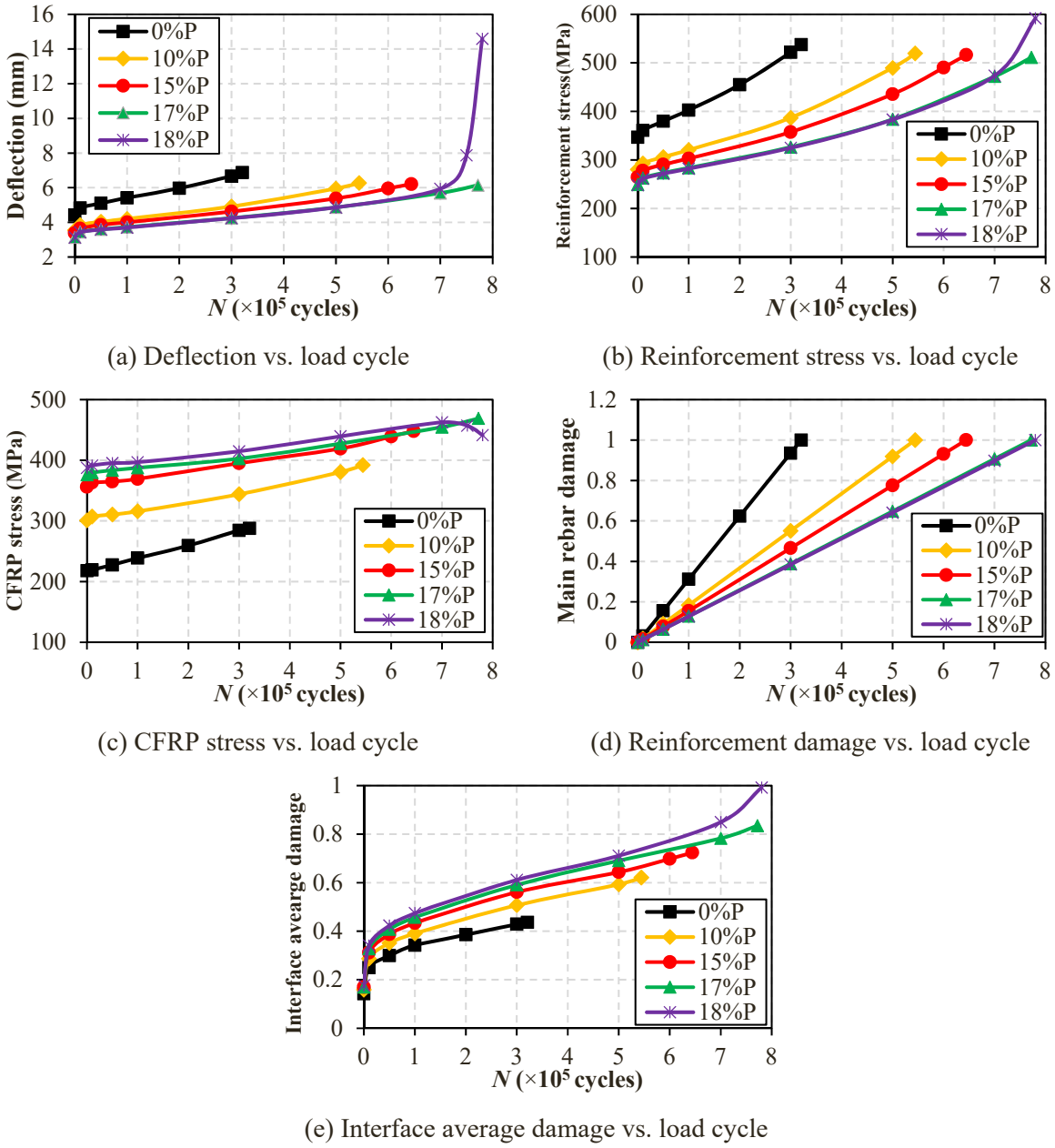

(a) Deflection vs. load cycle

(b) Reinforcement stress vs. load cycle

(c) CFRP stress vs. load cycle

(d) Reinforcement damage vs. load cycle

(e) Interface average damage vs. load cycle

Fig. 16. Fatigue analysis of prestressed SB-CFRP-strengthened beams.

interface reaches around 0.85, indicating that 85 % of the total length is affected by CFRP delamination. Subsequently, both peaks experience a significant surge in displacement growth at the first and second jump points, indicating rapid deterioration in the monitored fatigue damage and suggesting complete CFRP delamination. Notably, the second stage's displacement vibration response is smaller than the first. However, the change in frequency is notably greater, emphasizing the effectiveness of the method in detecting extensive delamination in prestressed CFRP-reinforced structures.

4.4. Analysis of natural frequency and stiffness degradation

Fig. 22 depicts changes in the natural frequencies of SB-CFRP-retrofitted beams during fatigue cycles at 0 %, 10 %, and 18 % prestress levels. Generally, applying prestress increases the first- and second-mode natural frequencies, with a more noticeable impact on the second mode. Prestress also induces a more gradual decline in natural frequencies over time, slowing down frequency degradation and delaying decline in later stages. However, higher prestress levels can accelerate frequency degradation due to increased CFRP delamination at the later fatigue stages.

The effects of prestress levels on the stiffness of prestressed SB-CFRP retrofitted beams are shown in Fig. 23. Prestress enhances stiffness and slows down degradation. For instance, at $N = 3 \times 10^5$ cycles, the stiffness reductions for beams with 0 %, 10 %, and 18 % prestresses are 36.1 %, 29.3 %, and 29.1 %, respectively. In later fatigue stages, extensive CFRP delamination significantly reduces stiffness. Beams with 18 % prestress experience a 73.9 % reduction in stiffness at $N = N_f$, while beams with 0 % and 10 % prestresses have reductions of 38.1 % and 46.7 % in stiffness, respectively.

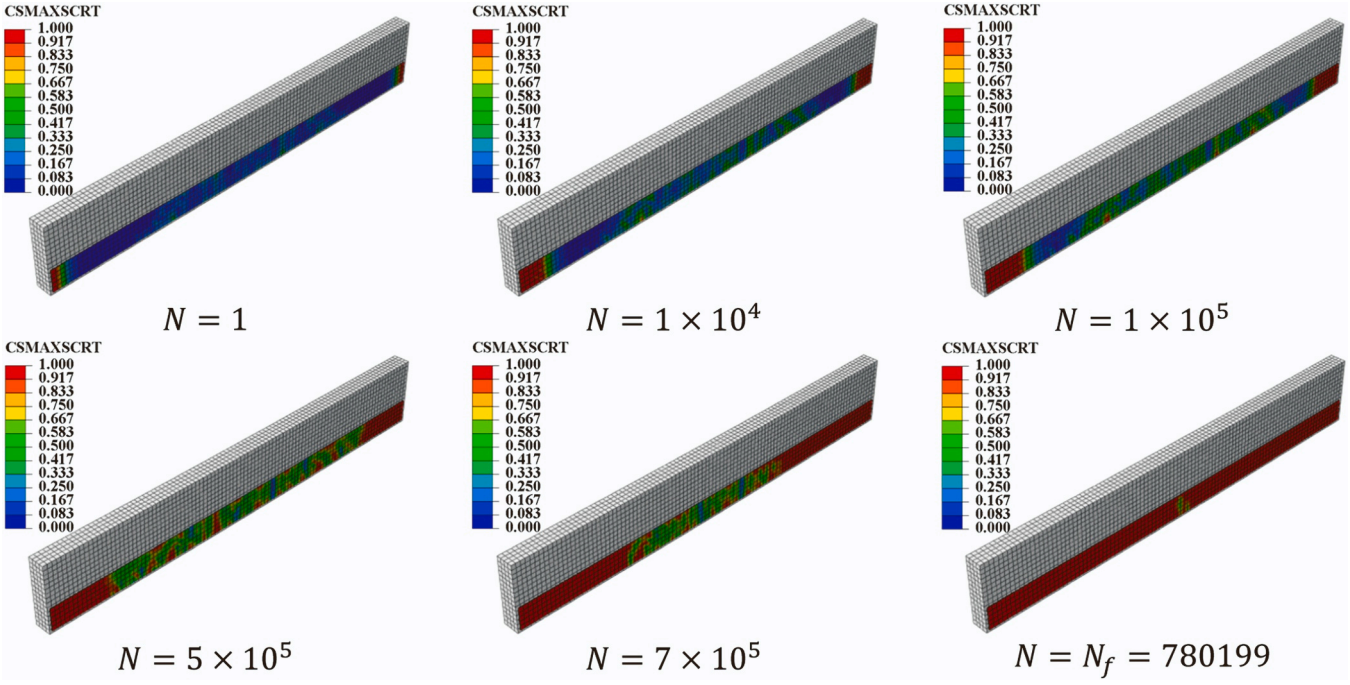

Fig. 17. Damage evolution of CFRP-concrete interface of SB-CFRP strengthened beams.

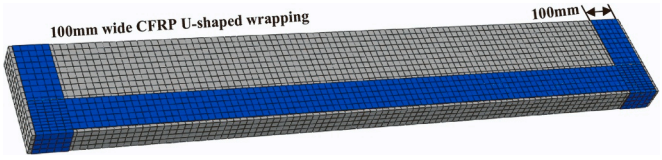

Fig. 18. SB-CFRP-reinforced beams with 100 mm wide U-shaped wrapping designed at ends.

5. Proposed fatigue life prediction model

5.1. P_{max}-N fatigue model

S-N curves are commonly used to describe the relationship between load levels and fatigue life and can be expressed as follows:

$$e^{\beta \cdot S} N = A \tag{19}$$

where S represents the load level, N represents the fatigue life, e is the natural logarithm, and β and A are constants.

It can be noticed from Eq. (19) that there is a logarithmic relationship between fatigue load S and fatigue life N, which is linearly related to the logarithmic form of fatigue life $\log_{10}N$. Hence, Eq. (19) can be represented as follows:

$$S = \frac{1}{\beta}\log_{10}A - \frac{1}{\beta}\log_{10}N = a + b\log_{10}N \tag{20}$$

where $a = \frac{1}{\beta}\log_{10}A$ and $b = -\frac{1}{\beta}$ are constants.

Following this principle, the least-squares method was used to fit the FE data for beams subjected to prestress levels of 0 %, 10 %, 15 %, and 18 % under four-point loading, as depicted in Fig. 24. It can be observed from Fig. 24 that all fitted data points fall within the 95 % confidence and prediction bands. The coefficient of determination (R^2) for the data fit ranges from 0.907 to 0.946, indicating an accurate representation of the data. The proposed model for P_{max}-N analysis, depicting the relationship between P_{max} and N, can thus be expressed as follows:

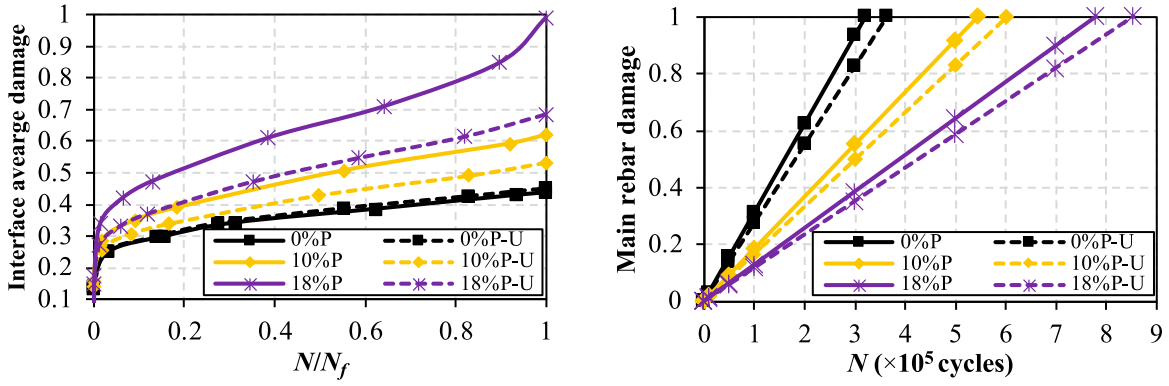

(a) CFRP-concrete interface damage (b) Steel reinforcement accumulated damage

Fig. 19. Evolution of interface damage and accumulated steel reinforcement damage of SB-CFRP-strengthened beams with U-shaped wrapping.

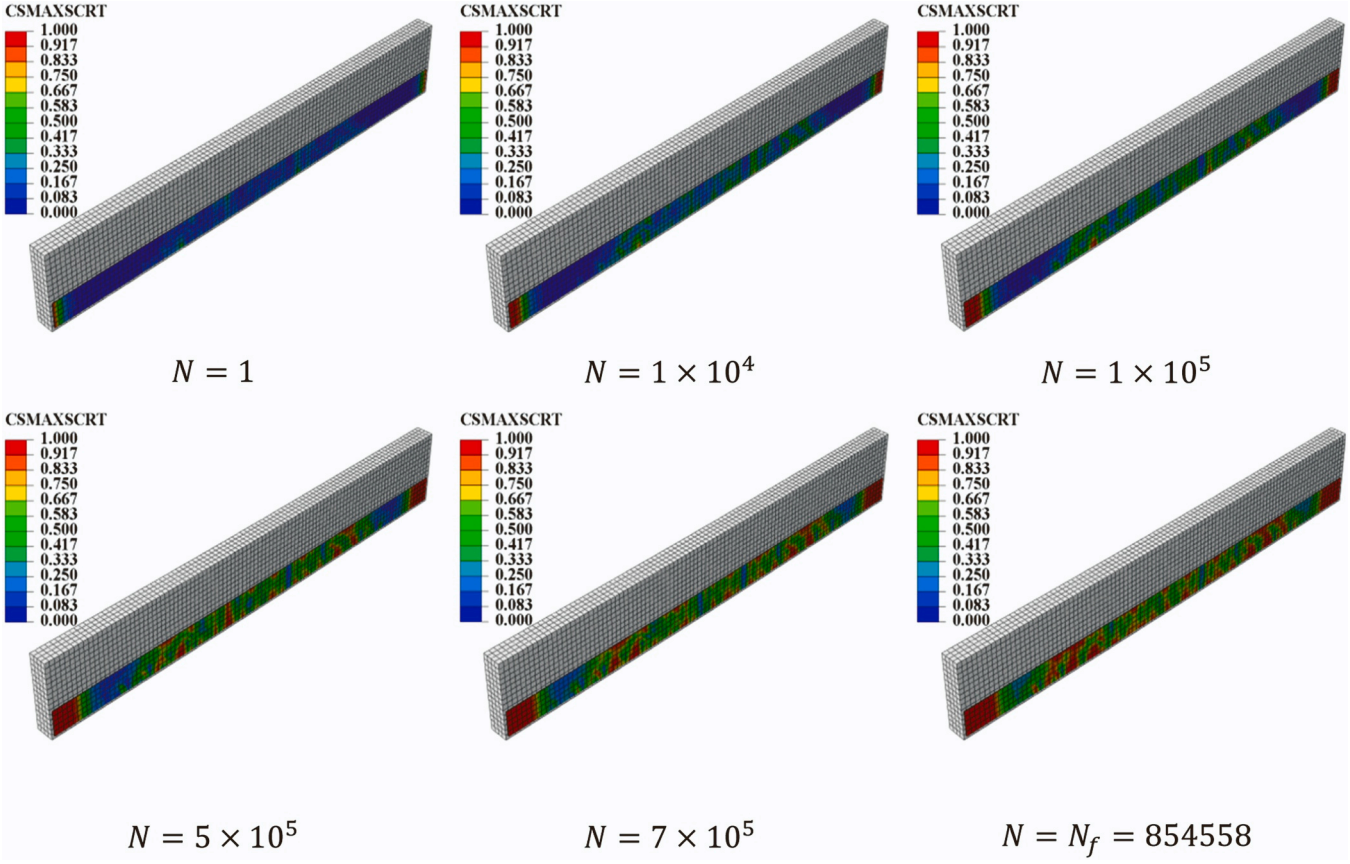

Fig. 20. Interface damage of SB-CFRP-strengthened beams with U-shaped wrapping.

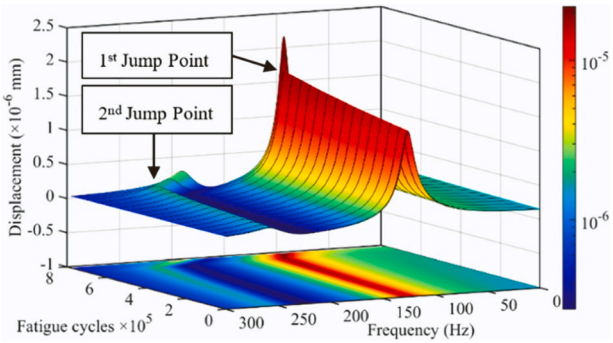

Fig. 21. Frequency-displacement vibration response.

$$P_{\max} = \begin{cases} 202.0273 - 15.2485\log_{10}N & for \quad \sigma_p/\sigma_{fu} = 0\% \\ 207.7744 - 15.6416\log_{10}N & for \quad \sigma_p/\sigma_{fu} = 10\% \\ 243.5058 - 21.0277\log_{10}N & for \quad \sigma_p/\sigma_{fu} = 15\% \\ 249.3248 - 21.5686\log_{10}N & for \quad \sigma_p/\sigma_{fu} = 18\% \end{cases} \tag{21}$$

where $P_{\max}$ and σ_p/σ_{fu} represent the load level and prestress level, respectively; σ_p and σ_{fu} denote the applied CFRP prestress value and CFRP's yield strength, respectively.

Likewise, in the case of three-point bending tests, utilizing the fatigue load test data obtained from the BB-CFRP-strengthened beams with prestress levels of 0 %, 15 %, and 22 % [38,74], a corresponding set of equations describing the P_{max} -N relationship can be formulated as follows:

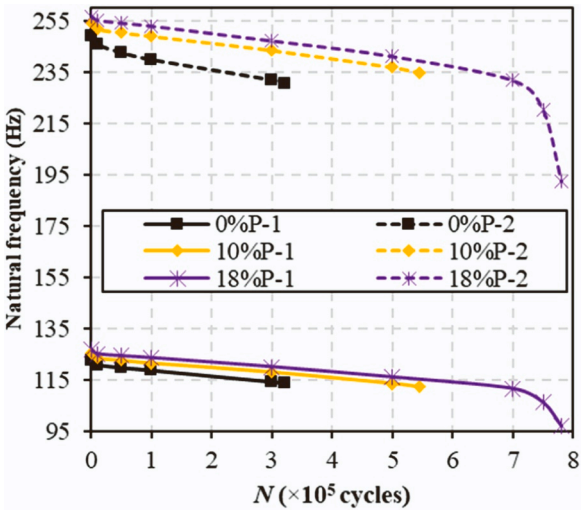

Fig. 22. Variation of natural frequency with cycles.

$$P_{\max} = \begin{cases} 68.1513 - 6.9272\log_{10}N & for \quad \sigma_p/\sigma_{fu} = 0\% \\ 91.5207 - 9.4203\log_{10}N & for \quad \sigma_p/\sigma_{fu} = 15\% \\ 91.2978 - 9.2474\log_{10}N & for \quad \sigma_p/\sigma_{fu} = 22\% \end{cases} \tag{22}$$

5.2. Simplified fatigue life prediction model and validation

It can be established that the logarithmic form of fatigue life $\log_{10}N$ correlates linearly with the fatigue peak load $P_{\max}$. This section establishes equations for $\log_{10}N$ based on prestress level and load level $P_{\max}$ to

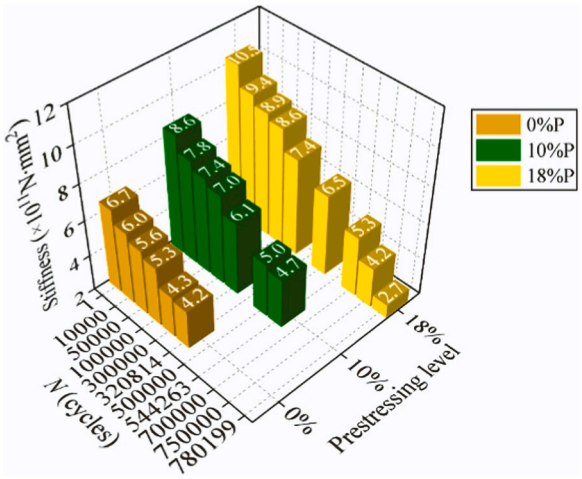

Fig. 23. Variation of stiffness with cycles.

simplify calculations. Using MATLAB and Eqs. (21) and (22), nonlinear fits were separately conducted for four-point bending fatigue analysis of SB-CFRP-strengthened beams and three-point bending fatigue tests of BB-CFRP-strengthened beams [21,59]. These fits were performed within the fatigue limit defined by ACI 215R-74 [78] as $P_f = P_{\max|N=2\times10^6}$. The outcomes of these fits are shown in Fig. 25.

It can be seen from Fig. 25 that the determination coefficients (R^2) for the data fitting of SB-CFRP and BB-CFRP-strengthened beams [38,74] are 0.9923 and 0.9843, respectively. This indicates that the fitting models effectively capture the variability in the data. Small square errors (SSE) suggest minimal discrepancies between models and actual data. Root Mean Square Error (RMSE) values of 0.1587 and 0.2371 are relatively low, indicating negligible differences between model predictions and actual observations. Overall, based on numerical calculations and experimental data [38,74], the proposed models (Eqs. (23) and (24)) exhibit exceptional fit, demonstrating high accuracy and explanatory capability.

$$\log_{10}N = 13.5768 - 0.0686P_{\max} - 11.5248\sigma_p/\sigma_{fu} + 0.1247P_{\max}\sigma_p/\sigma_{fu} \quad (23)$$

$$\log_{10}N = 9.5770 - 0.1340P_{\max} + 1.2355\sigma_p/\sigma_{fu} + 0.1386P_{\max}\sigma_p/\sigma_{fu} \quad (24)$$

It should be noted that Eq. (23) is for beams with SB-CFRP sheets and Eq. (24) is for beams with BB-CFRP strips. The accuracy of the proposed model is confirmed by comparing $\log_{10}N$ predictions from Eqs. (23) and (24) with FE analysis and experimental results [38,74] in Table 5. The model consistently predicts $\log_{10}N$ with an average ratio of 0.97 compared to FE analysis and 0.99 compared to experimental data. This implies that the proposed model gives precise prediction of the fatigue life of RC beams strengthened with CFRP sheets under various prestress and load levels.

In summary, by defining coefficients in Eqs. (23) and (24), a fatigue life prediction equation for CFRP-strengthened beams under the combined action of fatigue load and prestress can be formulated as follows:

$$\log_{10}N = a + bP_{\max} + c\sigma_p/\sigma_{fu} + dP_{\max}\sigma_p/\sigma_{fu} \quad (25)$$

where a, b, c, and d represent constants related to the fatigue load level

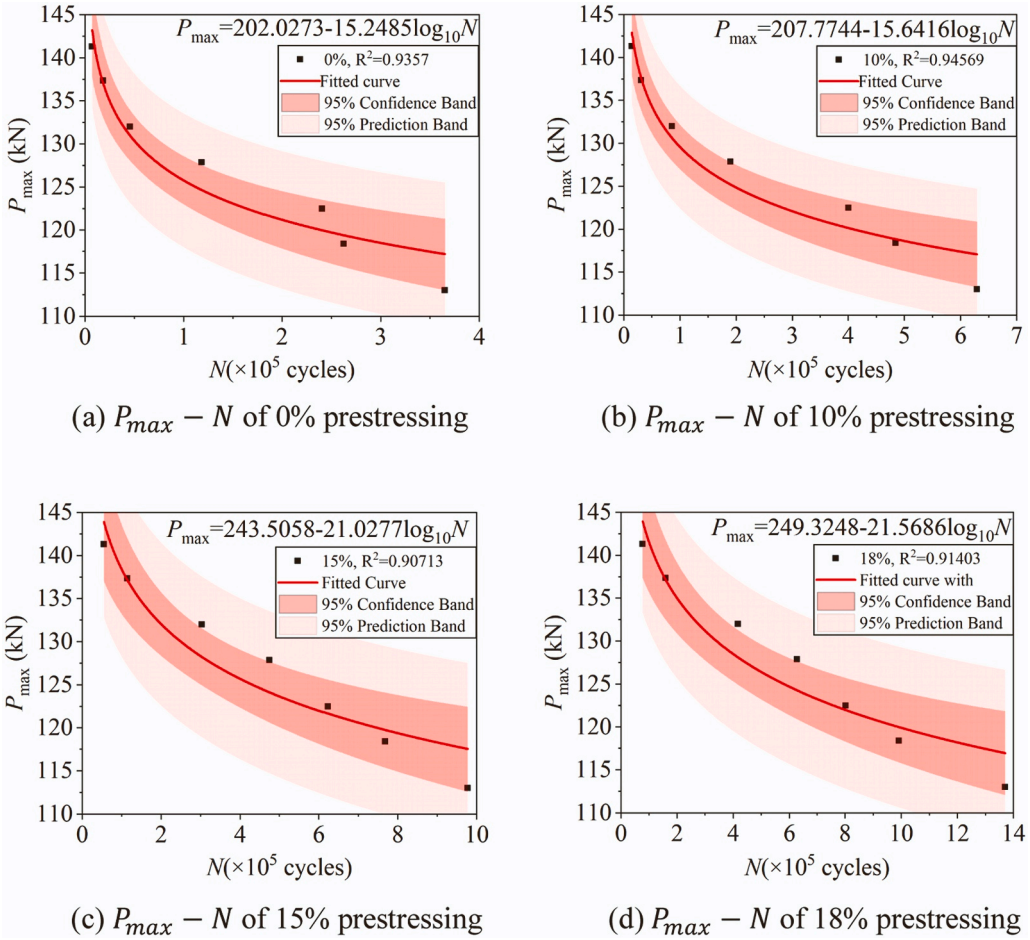

Fig. 24. Fatigue life prediction for different prestressed SB-CFRP-strengthened beams.

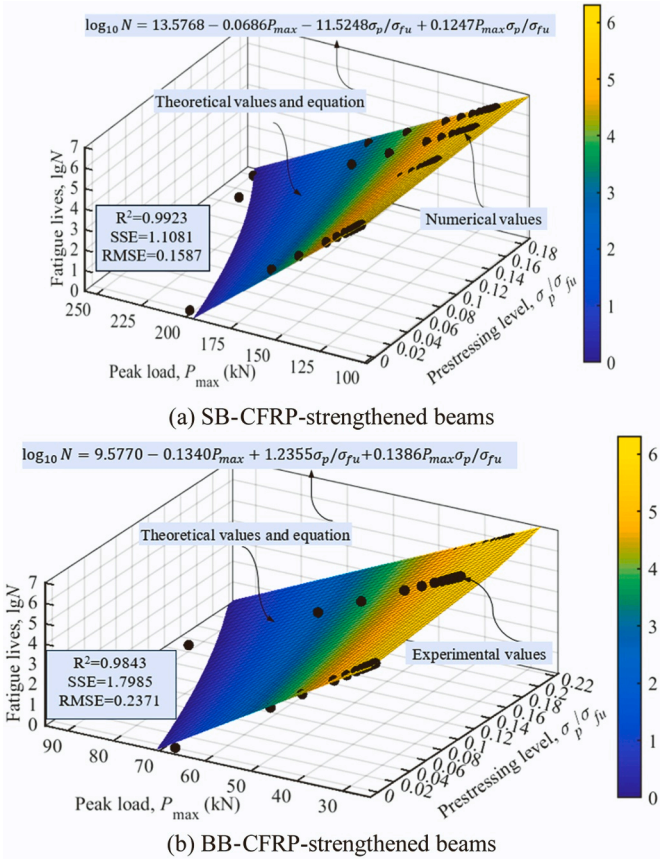

Fig. 25. The relationship between fatigue load, prestress level, and fatigue life.

and prestress level.

5.3. Fatigue limit analysis

In practical engineering applications, the fatigue performance of conventional RC structures is frequently assessed using the fatigue limit defined by ACI 215R-74 [78]. A similar method was used by Lin et al. [8, 82] and Huang [74] for developing a model to predict the fatigue limit of RC beams strengthened with CFRP sheet. Consequently, by substituting $N = 2 \times 10^6$ into Eq. (23), the relationship between the fatigue limit P_f of SB-CFRP-reinforced beams and the prestress level (σ_p/σ_{fu}) can be derived as follows:

$$P_f = (7.2758 - 11.5248\sigma_p/\sigma_{fu})/(0.0686 - 0.1247\sigma_p/\sigma_{fu}) \quad (26)$$

Fatigue limits of prestressed SB-CFRP-reinforced beams under the same load, determined using Eq. (26), show an escalation with higher prestress levels. For instance, at 0 %, 10 %, 15 %, and 18 % prestress, predicted fatigue load limits P_f are 106 kN, 109 kN, 111 kN, and 113 kN, respectively. Consequently, under the same fatigue load, increasing the prestress level leads to an increase in fatigue life.

Fig. 26 displays a contour plot for SB-CFRP-reinforced beams, depicting the correlation between fatigue load and prestress level over $\log_{10}N$ values ranging from 0 to 6.301, (N values from 1 to 2 $\times 10^6$ cycles). Notably, fatigue load rises with increasing prestress level at the same cycle count, with a more pronounced rate in the early fatigue stages, gradually stabilizing near the fatigue limit. Additionally, higher prestress levels enhance fatigue life under the same applied load, emphasizing the substantial influence of loading conditions on the fatigue behavior of SB-CFRP-reinforced beams.

6. Conclusions

A finite element model has been presented in this paper for predicting the fatigue responses of RC beams that are externally strengthened by using side-bonded CFRP sheets. The cycle-dependent degradation of the CFRP-concrete interface under fatigue loading is considered in the formulation. The FE model has been employed to investigate the fatigue behavior of strengthened RC beams incorporating CFRP strips with various design parameters, including CFRP dimensions, fatigue and prestress levels, and U-shaped wrapping. Based on the experimental and numerical results, a fatigue life prediction model has been proposed for RC beams strengthened with SB-CFRP strips.

The following conclusions are drawn from this study:

(1) The strengthened beams' deflection, main reinforcement stress, cumulative damage, and CFRP-concrete interface damage are notably affected by CFRP width and load levels. Primary failure modes in SB-CFRP-strengthened beams vary, with steel bar fracture or concrete failure depending on CFRP width and load levels.
(2) Prestressing diminishes fatigue deflection and cumulative damage in SB-CFRP-strengthened beams, prolonging their service life.
(3) Adding U-shaped wrapping at beam ends effectively mitigates debonding failure in SB-CFRP systems. This strategy reduces damage at the CFRP-concrete interface, delays cumulative damage in the main reinforcement, and is efficient in high prestress scenarios.
(4) Over fatigue cycles, SB-CFRP-strengthened beams experience a decrease in natural frequencies and stiffness. Prestressing, compared to non-prestressed beams, enhances these properties, slowing their degradation. However, excessive prestress levels may accelerate the decline, particularly in later fatigue stages.
(5) A fatigue life prediction equation for externally bonded CFRP-strengthened RC beams considering the linear relationship between P_{max} and $\log_{10}N$ in the S-N was proposed. The equation accurately predicts fatigue life and limit for SB CFRP-strengthened RC beams, offering vital theoretical guidance for structure assessment and design.

CRediT authorship contribution statement

Chuanlong Zou: Writing – review & editing, Writing – original draft, Software, Methodology, Investigation, Formal analysis, Data curation, Conceptualization. **Pouria Ayough:** Writing – review & editing, Writing – original draft, Supervision, Methodology, Investigation, Formal analysis. **Qing Quan Liang:** Writing – review & editing, Supervision, Methodology. **Huzaifa Hashim:** Writing – review & editing, Supervision, Methodology, Investigation. **Zainah Ibrahim:** Writing – review & editing, Writing – original draft, Supervision, Methodology, Investigation, Funding acquisition, Formal analysis, Conceptualization. **Mohammed Jameel:** Writing – review & editing, Formal analysis, Data curation.

Declaration of Competing Interest

The authors whose names are listed immediately below certify that they have NO affiliations with or involvement in any organization or entity with any financial interest (such as honoraria; educational grants; participation in speakers' bureaus; membership, employment, consultancies, stock ownership, or other equity interest; and expert testimony or patent-licensing arrangements), or non-financial interest (such as personal or professional relationships, affiliations, knowledge or beliefs) in the subject matter or materials discussed in this manuscript.

Table 5
Comparison of the predicted fatigue life $\log_{10}N$ with the experimental results.

Model	Prestressing level σ_p/σ_{fu}	Peak load P_{max} (kN)	Valley load P_{min} (kN)	Fatigue lives $\log_{10}N$		Predicted/Test	Mean	SD	CoV
				Test	Prediction				
FE	16 %	118.40	35.52	5.928	5.97	1.00	0.975	0.0521	0.0534
		122.50	36.75	5.828	5.773	0.99			
		137.34	41.20	4.917	5.051	1.03			
	14 %	118.40	35.52	5.843	5.908	1.01			
		122.50	36.75	5.752	5.698	0.99			
		137.34	41.20	5.429	4.939	0.90			
	13 %	118.40	35.52	5.803	5.875	1.01			
		122.50	36.75	5.718	5.660	0.99			
		137.34	41.20	4.917	4.883	0.99			
	12 %	118.40	35.52	5.762	5.843	1.01			
		122.50	36.75	5.677	5.623	0.99			
		137.34	41.20	5.335	4.827	0.90			
	11 %	118.40	35.52	5.727	5.811	1.01			
		122.50	36.75	5.638	5.586	0.99			
		137.34	41.20	5.291	4.771	0.90			
	9 %	118.40	35.52	5.648	5.746	1.01			
		122.50	36.75	5.559	5.511	0.99			
		137.34	41.20	5.230	4.659	0.89			
	8 %	118.40	35.52	5.608	5.714	1.02			
		122.50	36.75	5.545	5.473	0.98			
		137.34	41.20	5.203	4.603	0.88			
	7 %	118.40	35.52	5.561	5.681	1.02			
		122.50	36.75	5.468	5.436	0.99			
		137.34	41.20	5.174	4.547	0.88			
	6 %	118.40	35.52	5.530	5.649	1.02			
		122.50	36.75	5.446	5.398	0.99			
		137.34	41.20	5.168	4.491	0.87			
	5 %	118.40	35.52	5.480	5.616	1.02			
		122.50	36.75	5.412	5.360	0.99			
		137.34	41.20	4.422	4.435	1.00			
Exp.[38,74]	10 %	30.00	6.00	6.361	6.096	0.96	0.996	0.0555	0.0557
		32.50	6.50	5.835	5.796	0.99			
		35.00	7.00	5.694	5.496	0.97			
		40.00	8.00	5.230	4.895	0.94			
	8 %	25.00	5.00	6.301	6.603	1.05			
		30.00	6.00	5.556	5.988	1.08			

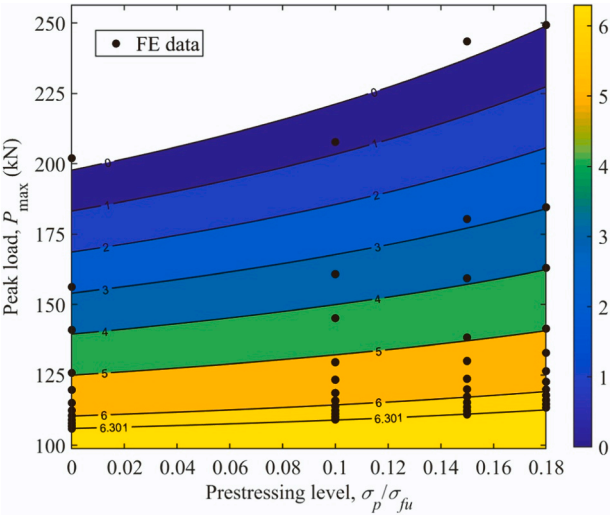

Fig. 26. Relationship between fatigue load and prestress level.

Data Availability

Data will be made available on request.

Acknowledgments

The authors would like to acknowledge the support of the Ministry of Higher Education, Malaysia, through the Fundamental Research Grant Scheme (FRGS/1/2020/TK0/UM/02/27), Basic Ability Improvement Project for Young and Middle-aged Teachers in Colleges and Universities in Guangxi (2022KY1776), China. In addition, the authors extend their appreciation to the deanship of scientific research at King Khalid University for funding this work through large group project under grant number (RGP. 2/94/44).

References

[1] Gudonis E, Timinskas E, Gribniak V, Kaklauskas G, Arnautov AK, Tamulėnas V. Frp reinforcement for concrete structures: state-of-the-art review of application and design. Eng Struct Technol 2014;5:147–58.
[2] Chen Z, Huang P, Yao G, Guo X, Yang Y, Li W, et al. Experimental study on fatigue performance of RC beams strengthened with CFRP under variable amplitude overload and hot-wet environment. Compos Struct 2020;244:112308.
[3] Kobatake Y, Kimura K, Katsumata H. A retrofitting method for reinforced concrete structures using carbon fiber. In: Nanni A, editor. In Fiber-Reinforced-Plastic (FRP) Reinforcement for Concrete Structures. Oxford: Elsevier; 1993. p. 435–50.
[4] Zou C, Ibrahim Z, Hashim H, Jameel M, Ayough P, Sinoh SS. Nonlinear FE analysis of RC slabs strengthened with prestressed EB CFRP strips under high-cyclic fatigue loading. Structures 2023;56:104953.
[5] Zhou H, Zhang SS, Fernando D, Huang T. The bond-behaviour of CFRP-to-concrete bonded joints under fatigue loading: a damage accumulation model. Eng Fract Mech 2023;284.
[6] Mahal M, Täljsten B, Blanksvärd T. Experimental performance of RC beams strengthened with FRP materials under monotonic and fatigue loads. Constr Build Mater 2016;122:126–39.
[7] Oehlers DJ, Park SM, Mohamed Ali MS. A structural engineering approach to adhesive bonding longitudinal plates to RC beams and slabs. Compos Part A: Appl Sci Manuf 2003;34:887–97.
[8] Lin J, Huang P, Guo Y, Guo X, Zeng J, Zhao C, et al. Fatigue behavior of RC beams strengthened with CFRP laminate under hot-wet environments and vehicle random loads coupling. Int J Fatigue 2020;131:105329.

[9] Chou J, Liu Y, Guo H, Zhang J, Peng H. Fatigue behavior of reinforced concrete beams strengthened with prestressed near-surface-mounted carbon-fiber-reinforced polymer strips. Compos Struct 2023;308:116689.
[10] Oudah F, El-Hacha R. Performance of RC beams strengthened using prestressed NSM-CFRP strips subjected to fatigue loading. J Compos Constr 2012;16:300–7.
[11] Oudah F, El-Hacha R. Fatigue behavior of RC beams strengthened with prestressed NSM CFRP rods. Compos Struct 2012;94:1333–42.
[12] Yost J., Gross S., Deitch M.: Fatigue behavior of concrete beams strengthened in flexure with near surface mounted CFRP. Proceedings of the 8th international symposium on fiber reinforced polymer reinforcement for reinforced concrete structures (FRPRCS8) 2007.
[13] Quattlebaum JB, Harries KA, Petrou MF. Comparison of three flexural retrofit systems under monotonic and fatigue loads. J Bridge Eng 2005;10:731–40.
[14] Wahab N, Soudki KA, Topper T. Mechanics of bond fatigue behavior of concrete beams strengthened with NSM CFRP rods. J Compos Constr 2011;15:934–42.
[15] Song L, Yu Z. Fatigue performance of corroded reinforced concrete beams strengthened with CFRP sheets. Constr Build Mater 2015;90:99–109.
[16] Wang Y, Guo X, Huang P, Huang K, Yang Y, Chen Z. Finite element investigation of fatigue performance of CFRP-strengthened beams in hygrothermal environments. Compos Struct 2020;234:111676.
[17] Zhang Y, Duan L, Liu H, Lu J, Huo Y. Experimental and numerical study on multi-impact performance of pre-damaged beams strengthened with CFRP. Eng Struct 2023;285:116034.
[18] Li X, Deng J, Liu Z, Zhu M, Luo S. Cracking behavior of prestressed CFRP strengthened RC beams subjected to wetting/drying cycling under flexural load. Constr Build Mater 2023;398:132403.
[19] Nawaz W, Hawileh RA, Saqan EI, Abdalla JA. Effect of longitudinal carbon fiber-reinforced polymer plates on shear strength of reinforced concrete beams. Acids Struct J 2016;113:577–86.
[20] Al-Tamimi AK, Hawileh RA, Abdalla JA, Rasheed HA, Al-Mahaidi R. Durability of the bond between CFRP plates and concrete exposed to harsh environments. J Mater Civ Eng 2015;27:04014252.
[21] Salama ASD, Hawileh RA, Abdalla JA. Performance of externally strengthened RC beams with side-bonded CFRP sheets. Compos Struct 2019;212:281–90.
[22] Li GB, Guo YG, Sun XY. Investigation on flexural performance of RC beams flexurally strengthened by soffit-bonding and side-bonding CFRP sheets. Adv Mater Res 2011;284-286:2521–5.
[23] Hawileh RA, Musto HA, Abdalla JA, Naser MZ. Finite element modeling of reinforced concrete beams externally strengthened in flexure with side-bonded FRP laminates. Compos Part B: Eng 2019;173:106952.
[24] Hosen MA, Jumaat MZ. Islam ABMS: Side Near Surface Mounted (SNSM) technique for flexural enhancement of RC beams. Mater Des 2015;83:587–97.
[25] Zheng XH, Huang PY, Han Q, Chen GM. Bond behavior of interface between CFL and concrete under static and fatigue load. Constr Build Mater 2014;52:33–41.
[26] Zou C, Ibrahim Z, Hashim H, Jamadin A, Ayough P. Nonlinear analysis of reinforced concrete slabs under high-cyclic fatigue loading. J Mater Res Technol 2022;21:992–1012.
[27] Kent DC, Park R. Flexural members with confined concrete. J Struct Div 1971;97:1969–90.
[28] Jan Ove H. Fatigue of concrete by constant and variable amplitude loading. Acids Symp Publ 1982:75.
[29] Bennett E, Raju NK. Cumulative Fatigue Damage of Plain Concrete in Compression. London: Wiley-Interscience; 1971.
[30] El-Tawil S, Ogunc C, Okeil A, Shahawy M. Static and fatigue analyses of RC beams strengthened with CFRP laminates. J Compos Constr 2001;5:258–67.
[31] ACI Committee 318. Building Code Requirements for Structural Concrete. USA: American Concrete Institute; 2014. $3^{18}R–^{14}A$.
[32] Song YP, Wang HL, Jia JQ. Behavior of concrete under multi-axial fatigue loading. J Build Struct(Suppl Issue) 2008;29:260–5.
[33] Thomas TCH. Fatigue of plain concrete. Acids J Proc 1981;78:292–305.
[34] Zanuy C, de la Fuente P, Albajar L. Effect of fatigue degradation of the compression zone of concrete in reinforced concrete sections. Eng Struct 2007;29:2908–20.
[35] Sima JF, Roca P, Molins C. Cyclic constitutive model for concrete. Eng Struct 2008;30:695–706.
[36] Aslani F, Jowkarmeimandi R. Stress–strain model for concrete under cyclic loading. Mag Concr Res 2012;64:673–85.
[37] Wang X, Zhou C, Ai J, Petrů M, Liu Y. Numerical investigation for the fatigue performance of reinforced concrete beams strengthened with external prestressed HFRP sheet. Constr Build Mater 2020;237:117601.
[38] Guo X, Wang Y, Huang P, Chen Z. Finite element modeling for fatigue life prediction of RC beam strengthened with prestressed CFRP based on failure modes. Compos Struct 2019;226:111289.
[39] Beijing: China Architecture & Building Press; 2011.
[40] Feng XF, Song YP, Song YC. Ful-range nonlinear analysis of fatigue damage in prestressed concrete flexural members. J Dalian Univ Technol 2005;45(3):410–5.
[41] Dong YT, Ansari F, Karbhari VM. Fatigue performance of reinforced concrete beams with externally bonded CFRP reinforcement. Struct Infrastruct Eng 2011;7:229–41.
[42] Barsom JM, Rolfe ST. Fracture and Fatigue Control in Structures: Applications of Fracture Mechanics. West Conshohocken, PA.: ASTM; 1999.
[43] Hashin Z. Fatigue failure criteria for unidirectional fiber composites. J Appl Mech 1981.
[44] Wang X, Zhou C. Numerical investigation for the flexural strengthening of reinforced concrete beams with external prestressed HFRP sheets. Constr Build Mater 2018;189:804–15.
[45] De Lorenzis L, Fernando D, Teng J-G. Coupled mixed-mode cohesive zone modeling of interfacial debonding in simply supported plated beams. Int J Solids Struct 2013;50:2477–94.
[46] Guo X, Wang Y, Huang P, Shu S. Fatigue behavior of RC beams strengthened with FRP considering the influence of FRP-concrete interface. Int J Fatigue 2021;143:105977.
[47] Neto P, Alfaiate J, Almeida JR, Pires EB. The influence of mode II fracture on concrete strengthened with CFRP. Comput Struct 2004;82:1495–502.
[48] Lu XZ, Teng JG, Ye LP, Jiang JJ. Finite element analysis of intermediate crack-induced debonding in FRP strengthened RC beams engineering mechanics. ASCE 2006;26:85–93.
[49] Lu XZ, Teng JG, Ye LP, Jiang JJ. Bond–slip models for FRP sheets/plates bonded to concrete. Eng Struct 2005;27:920–37.
[50] He J, Xian G. Debonding of CFRP-to-steel joints with CFRP delamination. Compos Struct 2016;153:12–20.
[51] Yu T, Fernando D, Teng JG, Zhao XL. Experimental study on CFRP-to-steel bonded interfaces. Compos Part B: Eng 2012;43:2279–89.
[52] Guo D, Gao W-Y, Liu Y-L, Dai J-G. Intermediate crack-induced debonding in CFRP-retrofitted notched steel beams at different service temperatures: Experimental test and finite element modeling. Compos Struct 2023;304:116388.
[53] Liu M, Dawood M. A closed-form solution of the interfacial stresses and strains in steel beams strengthened with externally bonded plates using ductile adhesives. Eng Struct 2018;154:66–77.
[54] Stratford T, Bisby L. Effect of warm temperatures on externally bonded FRP strengthening. J Compos Constr 2012;16:235–44.
[55] Dehghani E, Daneshjoo F, Aghakouchak AA, Khaji N. A new bond-slip model for adhesive in CFRP–steel composite systems. Eng Struct 2012;34:447–54.
[56] Cornetti P, Carpinteri A. Modelling the FRP-concrete delamination by means of an exponential softening law. Eng Struct 2011;33:1988–2001.
[57] Zhou H, Fernando D, Thuan Nguyen V, Dai J-G. The bond behaviour of CFRP-to-concrete bonded joints under fatigue cyclic loading: An experimental study. Constr Build Mater 2021;273:121674.
[58] Daud RA, Cunningham LS, Wang YC. Static and fatigue behaviour of the bond interface between concrete and externally bonded CFRP in single shear. Eng Struct 2015;97:54–67.
[59] Tan KH. Effect of cyclic loading on FRP-concrete interface bond strength. In Proceedings of the International Symposium on Latest Achievement of Technology and Research on Retrofitting Concrete structures. Japan: Japan Concrete Institute; 2003. p. 1–8. 1-8.
[60] Wang W.W., Huang H.: Fatigue life prediction of RC beams strengthened with externally bonded FRP sheets. In International Conference on Performance-based and Life-cycle Structural Engineering. pp. 522–5282015:522–528.
[61] Maalej M, Leong K. Effect of beam size and FRP thickness on interfacial shear stress concentration and failure mode of FRP-strengthened beams. Compos Sci Technol 2005;65:1148–58.
[62] Nguyen DM, Chan TK, Cheong HK. Brittle failure and bond development length of CFRP-concrete beams. J Compos Constr 2001;5:12–7.
[63] Meng X, Liu Y, Ning Z, Dong J, Liang G, Wang Y. Fatigue performance of hydraulic asphalt concrete under uniaxial constant-amplitude tensile cycle loading. J Build Eng 2023;80:108070.
[64] Cui K, Xu L, Li X, Hu X, Huang L, Deng F, et al. Fatigue life analysis of polypropylene fiber reinforced concrete under axial constant-amplitude cyclic compression. J Clean Prod 2021;319:128610.
[65] Cui K, Xu L, Li L, Chi Y. Mechanical performance of steel-polypropylene hybrid fiber reinforced concrete subject to uniaxial constant-amplitude cyclic compression: Fatigue behavior and unified fatigue equation. Compos Struct 2023;311:116795.
[66] Du Y, Wei J, Yuan J, Lai Y, Sun D. Experimental research on fatigue behavior of prestressed concrete beams under constant-amplitude and variable-amplitude fatigue loading. Constr Build Mater 2020;259:119852.
[67] Li JZ. Study on Flexural Capacity of RC Beams Strengthened with Prestressed Carbon Fiber Laminate. ME Thesis. South China University of Technology; 2008.
[68] Al-Tamimi AK, Hawileh R, Abdalla J, Rasheed HA. Effects of ratio of CFRP plate length to shear span and end anchorage on flexural behavior of SCC RC beams. J Compos Constr 2011;15:908–19.
[69] Esfahani MR, Kianoush M, Tajari A. Flexural behaviour of reinforced concrete beams strengthened by CFRP sheets. Eng Struct 2007;29:2428–44.
[70] Obaidat YT, Heyden S, Dahlblom O, Abu-Farsakh G, Abdel-Jawad Y. Retrofitting of reinforced concrete beams using composite laminates. Constr Build Mater 2011;25:591–7.
[71] Sabzi J, Esfahani MR. Effects of tensile steel bars arrangement on concrete cover separation of RC beams strengthened by CFRP sheets. Constr Build Mater 2018;162:470–9.
[72] Huang KN. Numerical Simulation of Fatigue Behavior of RC Beams Strengthened with Prestressed CFRP under High Humid and Temperature Environment. ME Thesis. South China University of Technology; 2019.
[73] Xie JH. Study on flexural fatigue performance of RC Beams Strenthened with Prestressed CFL. PhD Thesis. South China University of Technology; 2009.
[74] Huang JL. Study on Fatigue Properties of RC Beams Strenthened with Pre-tensioned Prestressed CFL. PhD Thesis. South China University of Technology; 2014.
[75] Guo X, Huang K, Huang P, Zheng X, Zhao C. Fatigue crack propagation behaviour of RC beams strengthened with prestressed CFRP under cyclic bending loads. Fatigue Fract Eng Mater Struct 2019;42:480–93.

[76] Guo X, Yu B, Huang P, Zheng X, Zhao C. J-integral approach for main crack propagation of RC beams strengthened with prestressed CFRP under cyclic bending load. Eng Fract Mech 2018;200:465–78.
[77] Xie J, Huang P, Guo X. Analysis of debonding load-carrying capacity for RC beams strengthened with prestressed FPR under bending load. J South China Univ Technol(Nat Sci Ed) 2009;37(6):107–12.
[78] ACI Committee 215. Considerations for Design of Concrete Structures Subjected to Fatigue Loading. USA: American Concrete Institute; 1997. 215R-74 (92).
[79] Zheng S., Huang P., Guo X.Analysis on Fatigue Lives of RC Beams Strengthened with Prestressed FRP under Bending Loads. In *P*roceedings of the 19th National Structural Engineering Conference (Volume II); China2010: 233–237.
[80] Al-Rousan R, Issa M. Fatigue performance of reinforced concrete beams strengthened with CFRP sheets. Constr Build Mater 2011;25:3520–9.
[81] Wang YL, Guo XY, Shu SYH, Guo YC, Qin XM. Effect of salt solution wet-dry cycling on the bond behavior of FRP-concrete interface. Constr Build Mater 2020;254: 119317.
[82] Lin J. Fatigue performance of RC beams strengthened with CFRP under coupling action of hot-wet environment and vehicle random load. PhD Thesis. South China University of Technology; 2018.